SCIENCE CHINA
Physics, Mechanics & Astronomy

• Invited Review •

April 2026 Vol. 69 No. 4: 249501
https://doi.org/10.1007/s11433-025-2870-8

Towards realistic detection pipelines of Taiji: New challenges in data analysis and high-fidelity simulations of space-based gravitational wave antenna

Minghui Du[1*], Pengcheng Wang[2,3], Ziren Luo[1,4,5], Wen-Biao Han[4,6,7,8], Xin Zhang[9,10,11], Xian Chen[12,13], Zhoujian Cao[8,14,15], Yonghe Zhang[2], He Wang[4,16], Xiaodong Peng[8,17], Li-E Qiang[17], Ke An[2,3], Yidi Fan[2,3], Jiafeng Zhang[17], Liang-Gui Zhu[13], Ping Shen[6,8], Qianyun Yun[6,18,19], Xiao-Bo Zou[8], Ye Jiang[6,7], Tianyu Zhao[1], Yong Yuan[1], Xiaotong Wei[1], Yuxiang Xu[1], Bo Liang[1], Peng Xu[1,4,5,20*], and Yueliang Wu[16,18,21*]

[1] *Center for Gravitational Wave Experiment, National Microgravity Laboratory, Institute of Mechanics, Chinese Academy of Sciences, Beijing 100190, China*
[2] *Innovation Academy for Microsatellites of Chinese Academy of Sciences, Shanghai 201304, China*
[3] *Key Laboratory for Satellite Digitalization Technology, Chinese Academy of Sciences, Shanghai 201210, China*
[4] *Taiji Laboratory for Gravitational Wave Universe (Beijing/Hangzhou), University of Chinese Academy of Sciences (UCAS), Beijing 100049, China*
[5] *Key Laboratory of Gravitational Wave Precision Measurement of Zhejiang Province, Hangzhou Institute for Advanced Study, UCAS, Hangzhou 310024, China*
[6] *Shanghai Astronomical Observatory, Chinese Academy of Sciences, Shanghai 200030, China*
[7] *School of Astronomy and Space Science, University of Chinese Academy of Sciences, Beijing 100049, China*
[8] *School of Fundamental Physics and Mathematical Sciences, Hangzhou Institute for Advanced Study, UCAS, Hangzhou 310024, China*
[9] *Key Laboratory of Cosmology and Astrophysics (Liaoning) and College of Sciences, Northeastern University, Shenyang 110819, China*
[10] *National Frontiers Science Center for Industrial Intelligence and Systems Optimization, Northeastern University, Shenyang 110819, China*
[11] *Key Laboratory of Data Analytics and Optimization for Smart Industry (Ministry of Education), Northeastern University, Shenyang 110819, China*
[12] *Astronomy Department, School of Physics, Peking University, Beijing 100871, China*
[13] *Kavli Institute for Astronomy and Astrophysics, Peking University, Beijing 100871, China*
[14] *School of Physics and Astronomy, Beijing Normal University, Beijing 100875, China*
[15] *Institute for Frontiers in Astronomy and Astrophysics, Beijing Normal University, Beijing 102206, China*
[16] *International Centre for Theoretical Physics Asia-Pacific (ICTP-AP), UCAS, Beijing 100049, China*
[17] *Key Laboratory of Electronics and Information Technology for Space System, National Space Science Center, Chinese Academy of Sciences, Beijing 100190, China*
[18] *Hangzhou Institute for Advanced Study, University of Chinese Academy of Sciences, Hangzhou 310124, China*
[19] *School of Physics and Astronomy, Shanghai Jiao Tong University, Shanghai 200240, China*
[20] *Lanzhou Center of Theoretical Physics, Lanzhou University, Lanzhou 730000, China*
[21] *Institute of Theoretical Physics, Chinese Academy of Sciences, Beijing 100190, China*

Received June 14, 2025; accepted December 3, 2025; published online February 28, 2026

Taiji, a Chinese space-based gravitational wave (GW) detection project, aims to explore the millihertz GW universe with unprecedented sensitivity. By observing astrophysical and cosmological sources, including Galactic binaries, massive black hole binaries, extreme mass-ratio inspirals, and stochastic gravitational wave backgrounds, etc., Taiji is expected to deliver transformative insights into astrophysics, cosmology, and fundamental physics. However, Taiji's data analysis faces unique challenges

*Corresponding authors (Minghui Du, email: duminghui@imech.ac.cn; Peng Xu, email: xupeng@imech.ac.cn; Yueliang Wu, email: ylwu@itp.ac.cn)

compared to ground-based detectors like LIGO-Virgo-KAGRA, such as the overlap of numerous signals, extended data durations, more rigorous accuracy requirements for the waveform templates, incompletely characterized noise spectra, non-stationary noises, and various data anomalies. Taking Taiji as a representative example, this paper reviews the data characteristics and data analysis challenges of space-based GW detection, and introduces the second round of Taiji Data Challenge, a collection of simulation datasets designed as a shared platform for resolving these critical issues. This platform distinguishes itself from previous works by the systematic integration of orbital dynamics based on a full drag-free and attitude control simulation, extended noise sources, more complicated and overlapping GW signals, second-generation time-delay interferometry, and the coupling effect of time-varying arm-lengths, etc. Concurrently released is the open-source toolkit `Triangle` (available at https://github.com/TriangleDataCenter), which offers the capabilities for customized simulation of signals, noises, and other instrumental effects. By taking a step further towards realistic detection, Taiji Data Challenge II and `Triangle` altogether serve as a new testbed, supporting the development of Taiji's global analysis and end-to-end pipelines, and ultimately bridging the gaps between observation and scientific objectives.

space-based gravitational wave detection, numerical simulation, data analysis

Citation: M. Du, P. Wang, Z. Luo, W.-B. Han, X. Zhang, X. Chen, Z. Cao, Y. Zhang, H. Wang, X. Peng, L.-E Qiang, K. An, Y. Fan, J. Zhang, L.-G. Zhu, P. Shen, Q. Yun, X.-B. Zou, Y. Jiang, T. Zhao, Y. Yuan, X. Wei, Y. Xu, B. Liang, P. Xu, and Y. Wu, Towards realistic detection pipelines of Taiji: New challenges in data analysis and high-fidelity simulations of space-based gravitational wave antenna, Sci. China-Phys. Mech. Astron. **69**, 249501 (2026), https://doi.org/10.1007/s11433-025-2870-8

1 Introduction

In the last decade, the LIGO-Virgo-KAGRA (LVK) ground-based gravitational wave (GW) detection network [1-3] has opened a new era of astrophysics with the detection of over a hundred GW events in the Hz-kHz frequency band, originating from stellar-mass binary black holes, binary neutron stars, and black hole-neutron stars. More recently, in 2023, multiple international pulsar timing array (PTA) collaborations announced key evidence for nHz stochastic GW background (SGWB) [4-7], marking a major breakthrough in the detection of low-frequency GWs. Between these frequency regimes lies the mHz band, which is rich in both astrophysical and cosmological sources, and accessing this band is crucial for completing our understanding of the GW universe. Several ongoing space-based GW detection projects are designed to target the mHz band, including the Laser Interferometer Space Antenna (LISA) [8,9], Taiji [10-12], and TianQin [13], etc. [14,15].

LISA is currently the most established international space-based GW detection mission, which has already been approved by the European Space Agency to enter the engineering phase, preparing for the launch in 2035 [16]. Meanwhile, the Taiji project, initiated in 2008 by the Chinese Academy of Sciences (CAS), is also stated for launch in the 2030s [10,12]. The baseline design of Taiji comprises three spacecrafts (SCs) forming a triangular constellation with 3-million-kilometer arms. The constellation operates in a heliocentric orbit and leads the Earth by approximately 20°. As a recent milestone, Taiji-1, a technology demonstration satellite of Taiji [17], was launched in 2019 and had completed its mission to verify Taiji's key payloads and technologies, including laser interferometor [18], inertial sensor [19], micro thruster [20], drag-free control [21], and data processing [22,23], etc. Moreover, during its free fall, Taiji-1 also operated as a gravity recovery satellite and produced the global gravity model TJGM-r1911 [24]. All these advancements pave the path towards the final Taiji mission.

The scientific operation of Taiji will last for at least 5 years, during which it will be observing burst, continuous, and stochastic GW signals in the 0.1 mHz-1 Hz band, originating from various sources, including $O(10^7)$ extra-Galactic and Galactic binaries (GBs) ($O(10^4)$ resolvable, others forming a confusion foreground) [25], $O(10)$-$O(10^2)$ massive black hole binaries (MBHBs) [26,27], $O(1)$-$O(10^3)$ extreme mass-ratio inspirals (EMRIs, the number is inferred from the research on LISA [28]), the inspiral phase of $O(1)$-$O(10)$ stellar-mass black hole binaries (sBHBs) [29], as well as the astrophysical and/or cosmological SGWBs [30,31], etc.

Unlike the "noise-dominated" regime of LVK observations, the data of space-based detectors Taiji, LISA, and TianQin are anticipated as "signal-dominated", which exhibit several distinctive features. Firstly, as the signals overlap in both time and frequency domains, source-by-source analysis is generally impractical, making it inevitable to conduct joint analysis of multiple sources [32]. Secondly, a considerable fraction of signals have high signal-to-noise ratios (SNRs) up to $O(10^2)$-$O(10^3)$, thereby necessitating rigorous modeling of waveforms and detector responses [33]. Thirdly, the majority of detectable signals are continuous GWs with observation timescales of months to years (e.g., EMRIs, GBs), during which glitches, data gaps, and non-stationary noises

are anticipated to frequently occur [34]. Fourthly, the astrophysical confusion foreground and instrumental noises in space environments remain incompletely understood, and in the future in-orbit operational phase, we might not have the luxury to monitor and characterize noise properties with extra auxiliary methods [35]. Lastly, prior to scientific data analysis, data pre-processing constitutes a crucial stage for space-based GW detections, which undertakes the tasks of suppressing primary noises, calibrating key operational parameters, and assessing operational status and data quality, etc., with several of them inherently coupled with scientific analysis (see e.g., ref. [32]). Nevertheless, a comprehensive end-to-end data analysis pipeline from raw data to scientific outcomes remains unestablished. As will be detailed in Section 3, these features pose significant challenges unresolved by the conventional methodologies used in ground-based detections, and have been recognized internationally as critical problems in the field. The urgency for solving these challenges further intensifies with LISA's transition to the engineering phase and China's Taiji and TianQin missions pending approval.

Facing the limitations of traditional data analysis methods in disentangling overlapping signals and handling complex noises and anomalies, "Data Challenge" serves as a proactive strategy to discover and address the issues in advance. Based on the collaborative efforts of the Taiji simulation group, by creating mock datasets that encapsulate the complexity of Taiji's measurements, Taiji Data Challenge (TDC) aims to establish a standardized platform for the Taiji Scientific Collaboration and broader researchers to develop specialized algorithms and validate data analysis tools. TDC is expected to drive advancements in techniques and methodologies, including time-delay interferometry (TDI), Bayesian parameter estimation, machine learning, etc., hence playing a critical role in achieving Taiji's scientific objectives to reveal cosmic history, probe astrophysical phenomena, test fundamental theories, and unlock transformative insights into the dark universe.

In recent years, exploration has been made along this path, with well-known examples being the simulation datasets: mock LISA data challenge (MLDC) [36], LISA data challenge (LDC) [37], the first round of Taiji data challenge (TDC I) [38], as well as the multi-mission science data simulator for space-based GW detection `GWSpace` [39]. With the publication of "global analyses" on LDC2a by multiple groups [32,40-42], LDC has basically fulfilled its purpose as a simulation dataset based on simplified and idealized orbit configurations, instrumental noises, and GW waveforms. In view of the continuous development of the space-based GW detection missions, and the high-complexity of detector system that critically impacts GW detection and data analysis, we believe it is now necessary to take a further step to introduce more realities and complexities into the mock data of Taiji. Consequently, the second round of Taiji data challenge (TDC II) is released [43], aiming to explore and address the "new" challenges in the upcoming stage. Alongside mock datasets, an open-source toolkit "`Triangle`" used in the creation of TDC II will also be made public. `Triangle` is a prototype simulator for the data of space-based GW detectors. It offers visibility into the models behind TDC II and enables researchers to simulate a wide range of scenarios that go beyond the default settings of TDC II, hence supporting broader explorations on data analysis and GW sciences. Altogether, this new simulation testbed is anticipated to assist in bridging the gaps between Taiji's realistic observations and scientific objectives.

This paper is structured as follows: Section 2 outlines Taiji's mission design and scientific data flow. Taking Taiji as a representative example, Section 3 systematically reviews the key challenges for the data analysis of space-based GW detection. Motivated by these challenges, TDC II is introduced in Section 4, which includes 5 groups of datasets, each targeting specific topics listed in Section 3. The models and simulation framework used in mock data generation are also provided. Section 5 describes the open-source `Triangle` toolkit. The concluding remarks and outlooks for future development are presented in Section 6. The Appendix illustrates a simple parameter estimation task on the TDC II "verification" dataset using the tools provided in `Triangle`.

2 Basic mission designs and scientific data flow of Taiji

2.1 Baseline mission design for Taiji

As schematically shown in Figure 1, Taiji consists of three SCs configured in an approximate equilateral triangle constellation, with nominal arm-lengths of $\sim 3 \times 10^9$ m [10-12]. The constellation operates in a heliocentric orbit and leads the Earth by $\sim 20^\circ$.

The basic concepts and requirements for Taiji's systems and payloads are outlined in ref. [12]. In principle, the generation of mock data should stay faithful to these designs. The core systems relative to TDC II include the following.

Laser interferometry system Consisting of 1064 nm-wavelength lasers with 30 Hz/$\sqrt{\text{Hz}}$ frequency stability, 0.4 m-diameter telescopes with angular jitters of outgoing beams controlled at 1 nm/$\sqrt{\text{Hz}}$ level, and Michelson-type interferometers achieving pm/$\sqrt{\text{Hz}}$ precision via heterodyne detection [44]. In order to isolate the responses to GWs from the jitters of SCs, Taiji adopts the "split interferometry"

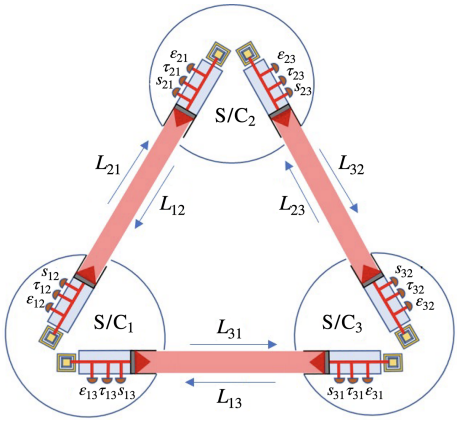

Figure 1 (Color online) A schematic diagram of Taiji constellation. Each SC is equipped with two movable optical sub-assemblies (MOSAs), which is a structure connecting a telescope, a gravitational reference sensor (GRS) that hosts a test-mass (TM), an optical bench carrying the laser sources, phasemeters, and other optical components needed for interferometric measurements, etc. Each MOSA is labeled by ij ($ij \in \{12, 23, 31, 21, 32, 13\}$), with i being the index of SC carrying this MOSA, and j the index of distant SC that transmits lasers with this MOSA. The indexing of on-board interferometric measurements $\{s_{ij}, \tau_{ij}, \varepsilon_{ij}\}$ are consistent with the MOSAs. For laser link L_{ij}, i, and j denote the SC that receives and emits laser, respectively.

design, which separates the interferometric measurements into inter-spacecraft interferometers (ISIs, or science interferometers, dubbed s_{ij}, see Figure 1 for the indexing convention of TDC II), reference interferometers (RFIs, τ_{ij}), and test-mass interferometers (TMIs, ε_{ij}). The TM-to-TM measurements η_{ij} used for GW detection are synthesized from them following two steps. Firstly,

$$\xi_{ij} = s_{ij} + \frac{\tau_{ij} - \varepsilon_{ij}}{2} + \mathbf{D}_{ij}\frac{\tau_{ji} - \varepsilon_{ji}}{2}, \tag{1}$$

where $ij \in \{12, 23, 31, 21, 32, 13\}$. The delay operator is defined as $\mathbf{D}_{ij}f(t) \equiv f[t - d_{ij}(t)]$, f being an arbitrary function of time, and $d_{ij}(t) \equiv L_{ij}(t)/c$ is the light travel time from SC_j to SC_i. Secondly,

$$\eta_{ij} = \xi_{ij} + \mathbf{D}_{ij}\frac{\tau_{ji} - \tau_{jk}}{2}, \quad \eta_{ik} = \xi_{ik} + \frac{\tau_{ij} - \tau_{ik}}{2}, \tag{2}$$

with $ijk \in \{123, 231, 312\}$. The sampling of the interferometric signals is triggered according to the onboard clocks, and the signals are ultimately measured by the phasemeters. Besides, the laser links also undertake functions such as clock noise transfering, inter-spacecraft ranging, and inter-spacecraft communications, etc. [45, 46].

Gravitational reference sensor (GRS) and drag-free and altitude control system (DFACS) Taiji employs 46-mm gold-platinum alloy TMs as free-falling inertial references, which are shielded in the GRSs, in order to isolate the TMs from non-gravitational disturbances from the space environment (e.g., solar radiation pressure). GRSs measure the displacements of SCs relative to TMs with capacitive sensing resolution of 1.8 nm/ $\sqrt{\mathrm{Hz}}$ along the sensitive axis and 3 nm/ $\sqrt{\mathrm{Hz}}$ along non-sensitive axes, feeding the readouts to the electrostatic servo control system of the GRS and the DFACS. The GRS controller will force the TMs to maintain its nominal positions along the non-sensitive axes, while the DFACS will command μN thrusters (force resolution 0.1 μN, noise 0.1 μN/ $\sqrt{\mathrm{Hz}}$, and response time < 0.33 s) to ensure that SC follows the trajectories of TMs along the sensitive axes. The residual displacement noise is required not to exceed nm/ $\sqrt{\mathrm{Hz}}$ level to reduce coupling stray forces. Meanwhile, the pointing ahead angle mechanism (PAAM) actively compensates for deviations from line of sight caused by orbital dynamics, and stabilizes laser alignment with angular jitter at the nrad/ $\sqrt{\mathrm{Hz}}$ order, maintaining robust laser link continuity. Under these controls, Taiji also requires that the breathing angles be within the scale of ±0.5° and the Doppler shifts between SCs be within ±5 MHz, during the whole mission lifetime. In principle, the full-scale simulation for GRS and DFACS entails up to 60 degrees of freedom, spanning the magnitudes from pm to astronomical unit [47].

In the raw measurements $\{s_{ij}, \tau_{ij}, \varepsilon_{ij}\}$, laser frequency noise, clock noise, and SC jitter dominate over the target GW signals by several orders of magnitude. These "primary" noises will be suppressed via split-interferometry design and the TDI data processing technique, thus the residual "secondary noises" ultimately determine the sensitivity of Taiji. As a preliminary categorization, Taiji's noise budget mainly comprises two components, one is the "position noise", which includes the contributions of multiple optical metrology system (OMS) noises, including shot noises and various optical path fluctuations, and the other is the test-mass acceleration (ACC) noise due to residual stray forces acting on the TMs. To enable GW observations in the 0.1 mHz-1 Hz band, the requirements on Taiji's OMS and ACC noises are $A_{\mathrm{OMS}} = 8$ pm/ $\sqrt{\mathrm{Hz}}$ and $A_{\mathrm{ACC}} = 3$ fm s^{-2}/ $\sqrt{\mathrm{Hz}}$, respectively, with spectral profiles designed as

$$P_{\mathrm{OMS}}(f) = A_{\mathrm{OMS}}^2\left[1 + \left(\frac{2\ \mathrm{mHz}}{f}\right)^4\right], \tag{3}$$

$$P_{\mathrm{ACC}}(f) = A_{\mathrm{ACC}}^2\left[1 + \left(\frac{0.4\ \mathrm{mHz}}{f}\right)^2\right]\left[1 + \left(\frac{f}{8\ \mathrm{mHz}}\right)^4\right], \tag{4}$$

where $P_{\mathrm{OMS}}(f)$ and $P_{\mathrm{ACC}}(f)$ denote the power spectral densities (PSDs) of OMS and ACC noises, respectively.

2.2 Taiji scientific data flow

After the data are downlinked to the Earth, the on-ground data processing flow transforms raw measurements into scientific outputs through a two-stage procedure. The design of this workflow draws inspiration from the research on Taiji, LISA, and TianQin, and incorporates the experiences gained

from Taiji-1. For clarity, we first introduce the definitions of data levels used in this work.

(1) Level 0 (L_0) data. Raw, unprocessed measurements downlinked from the SCs.

(2) Level 1 (L_1) data. Data processed through TDI to suppress the primary noises, resulting in TDI variables used by further scientific analysis.

(3) Level 2 (L_2) data. Output of the global fit pipeline, providing posterior parameter distributions for candidate GW sources.

(4) Level 3 (L_3) data. Final catalog of GW sources, astrophysical and cosmological parameters.

The two-stage processing workflow is as follows (see Figure 2 for a brief summary).

(1) The pre-processing stage (L_0 data $\rightarrow$ L_1 data, i.e., raw data to TDI outputs) aims to provide data that are suitable for scientific analysis, with primary noises effectively mitigated, and synchronized to a global time frame (e.g., the Barycentric Coordinate Time of Solar system, TCB for short). This stage includes inter-spacecraft ranging [45, 46, 48, 49], clock synchronization [50, 51], and the suppression of laser frequency noise [52-56], clock noise [57-60], SC jitter, tilt-to-length (TTL) coupling [61, 62] and other noises [63, 64] during or after the TDI processing. In a broader sense, it should also incorporate the calibration of key operating parameters of the science payloads and measurement links (e.g., the GRS scale factors, the bias of TM center-of-mass [23, 65], the thruster delay, etc), as well as the evaluation of their performances and data quality. As a critical step within pre-processing, TDI mitigates the laser frequency noise, which is predicted to be 6-8 orders of magnitude stronger than GW signals, by delaying and combining the raw interferometric measurements to synthesize virtual equal-arm-length interferometry. According to the ways of combination, TDI can be categorized into different configurations (i.e., TDI channels), such as the Michelson type, Sagnac type, Monitor type, Relay type, etc. [66, 67], or different generations, such as the 1st generation designed for static constellations, and the 2nd generation is more suitable for the flexing arm-lengths of LISA and Taiji. Regardless, all the TDI combinations can be written in a unified form

$$\mathrm{TDI} = \sum_{ij} \mathbf{P}_{ij}\eta_{ij}, \tag{5}$$

with $\mathbf{P}_{ij}$ synthesized from delay operators. For example, the rule of the Michelson-X_2 channel used in TDC II reads

$$\begin{aligned}
\mathbf{P}_{12} &= 1 - \mathbf{D}_{131} - \mathbf{D}_{13121} + \mathbf{D}_{1213131},\\
\mathbf{P}_{23} &= 0,\\
\mathbf{P}_{31} &= -\mathbf{D}_{13} + \mathbf{D}_{1213} + \mathbf{D}_{121313} - \mathbf{D}_{13121213},\\
\mathbf{P}_{21} &= \mathbf{D}_{12} - \mathbf{D}_{1312} - \mathbf{D}_{131212} + \mathbf{D}_{12131312},\\
\mathbf{P}_{32} &= 0,\\
\mathbf{P}_{13} &= -1 + \mathbf{D}_{121} + \mathbf{D}_{12131} - \mathbf{D}_{1312121},
\end{aligned} \tag{6}$$

where $\mathbf{D}_{i_1 i_2 i_3 \ldots} f(t) \equiv \mathbf{D}_{i_1 i_2}\mathbf{D}_{i_2 i_3}\ldots f(t)$.

(2) The scientific analysis stage (L_1 data $\rightarrow$ $L_{2,3}$ data, i.e., TDI outputs to source parameters and scientific interpreta-

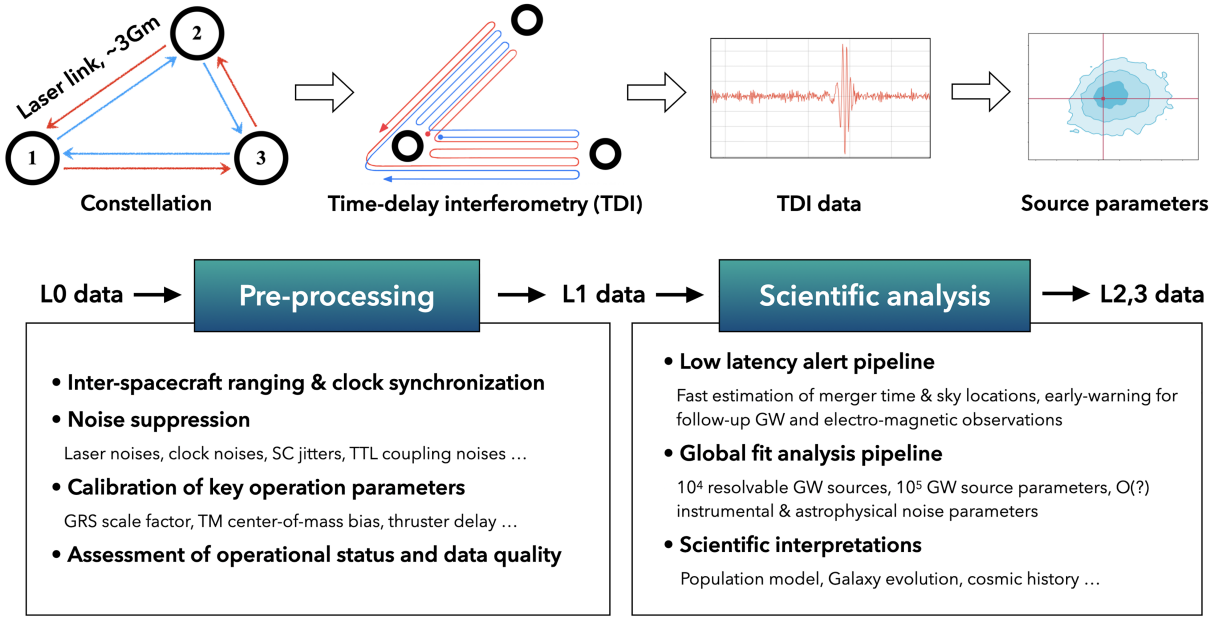

Figure 2 (Color online) The scientific data flow of Taiji.

tions) starts from the TDI data, and aims to accomplish the detection of GW signals, the estimation of source parameters, and further interpretation of GW physics. At least two pipelines play critical roles in this stage. One is the "low latency" alert pipeline [68-72], a real-time processing system designed to rapidly detect and locate transient GW events, enabling timely electromagnetic follow-up observations as well as potential multi-mission (e.g., LISA-Taiji [73, 74], LISA-Taiji-TianQin [15, 75] networks) and multi-band GW observations. The other is the "global fit" analysis pipeline [32, 40, 41], which performs computationally intensive Bayesian analysis to disentangle overlapping GW signals, precisely estimating the parameters of thousands of sources, and generating high-confidence source catalogs [76].

3 Challenges in Taiji data analysis

This section presents a systematic review of the anticipated challenges in future data analysis. Several demonstrations based on our simulation are provided in Figures 3-6. Given the similarities between Taiji and LISA in terms of mission concept, target sources, and sensitivity, the issues discussed here are relevant to both missions, and we expect this work to support the development of algorithms and tools with broad applicability across similar detectors.

3.1 The challenges of signal modeling and computational demand

Matched filtering is one of the most classical and well-established algorithms in GW data analysis [77, 78], and its implementation necessitates the accurate and efficient modeling of signals (i.e., templates). On the one hand, for a single GW event, Bayesian parameter estimation typically involves more than $O(10^6)$ template evaluations to sample high-dimensional posterior distributions [79]. On the other hand, high accuracy is also crucial to ensure that the templates can precisely match the actual GW signals, thereby maximizing the detection efficiency and minimizing false positives and biased estimation. These demands are also shared by machine learning methods such as simulation-based inference [79, 80], since they rely on the forward models of signals to generate large training sets. The template for GW signal comprises two aspects: waveform (polarizations) and detector response (single-link response and TDI combination). Achieving both speed and accuracy can be a challenging task, especially in the context of space-based GW detection.

A variety of quantitative criteria have been raised to assess and limit the accuracy of templates [81, 82], such as the mismatch threshold [83, 84], the parameter estimation error based on Fisher formalism [85], etc. A key observation is that higher-SNR signals generally demand more precise templates to avoid biased estimation, since for high SNRs, systematic errors can easily dominate statistical uncertainties. Among the target sources of Taiji and LISA, MBHBs can achieve SNRs of $O(10^3)$, and SNRs of $O(10^2)$ are also foreseen for bright GBs. The overlap of signals further exacerbates these requirements. For instance, the matching residual of one signal can potentially disrupt the accurate resolution of others. Meanwhile, this also indicates that subdominant features in the waveforms, such as the eccentricity [86], high harmonics beyond the dominant $(2, 2)$ mode [87, 88] (see Figure 3 for an illustrative example), and precession [89] of MBHB, as well as the eccentricity of GB [90], would become non-negligible. These complexities pose both theoretical and computational challenges for data analysis; while, the incorporation of these features could be beneficial for testing general relativity and exploring GW astrophysics [91, 92].

For space-based detections, the detector responses to GW signals diverge from those of LVK in at least two aspects. Firstly, the rotation and translation of the detector constellation induce time-dependent antenna pattern functions and Doppler effects, respectively. While these effects complicate response modeling, they also help to alleviate the degeneracies among extrinsic parameters, thereby enhancing the accuracy of source localization [93]. Secondly, the configurations

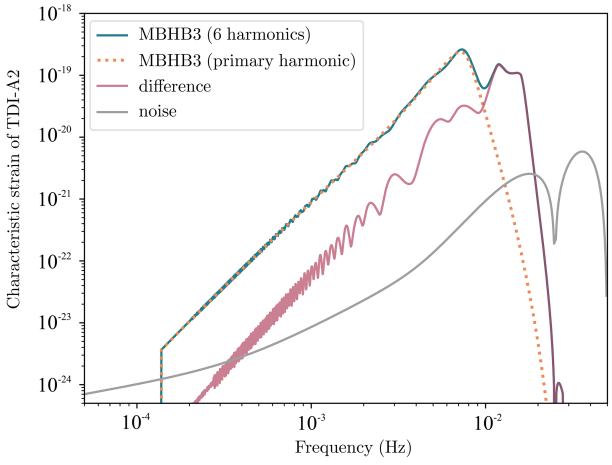

Figure 3 (Color online) Detectability of the higher harmonics, showcased using the parameters of the 3rd MBHB from dataset 1.1. The green solid curve represents the waveform (in terms of TDI-X_2 response) containing only the dominant (2,2) mode, while the orange dotted curve incorporates 6 harmonic modes: (2,1), (3,3), (3,2), (4,4), and (4,3). Systematic deviations caused by neglecting higher modes are quantified by the residual (yellow line), compared against the instrument noise floor (gray curve), defining the detection threshold. This mismatch necessitates the inclusion of higher modes for unbiased parameter estimation in the high-SNR regime.

of TDI combination, as well as the arm-length information (used as delays), also shape the response formalism. Current studies, particularly those targeting LDC, predominantly utilize 1st-generation Michelson TDI configurations under the equal-arm-length approximation. However, these frameworks become insufficient when applied to realistic Taiji/LISA orbits, where arm-lengths vary at rates up to several m/s. Therefore, it is imperative to employ 2nd-generation TDI configurations and account for dynamic arm-lengths. Ref. [94] demonstrated that, for high-SNR GBs ($O(10^2)$), using the idealistic equal-arm-length analytic orbit in response modeling would induce significant systematic biases in parameter estimation. Applying the same investigation to MBHBs with SNR $O(10^3)$, the resulting systematic deviations for both intrinsic and extrinsic parameters exceed the 3σ thresholds (see Figure 4).

Except for the stringent accuracy requirements, long-duration GW signals pose significant computational challenges due to the large data size (e.g., $O(10^6)$ data points per year for a sampling rate of 0.1 Hz). Although semi-monochromatic signals (e.g., GBs) can be efficiently calculated in the frequency-domain [95], chirping signals with time-frequency evolution, such as sBHB inspirals in the mHz-band which undergo significant frequency evolution over years, render traditional methods inadequate [96-99]. The EMRI waveforms, on the other hand, besides sharing the computational bottlenecks with sBHBs in template volume, face unique challenges due to their extreme complexity. To extract the wealth of GW science from observation, a sub-radian accuracy in phase (more specifically $\Delta\Phi <$

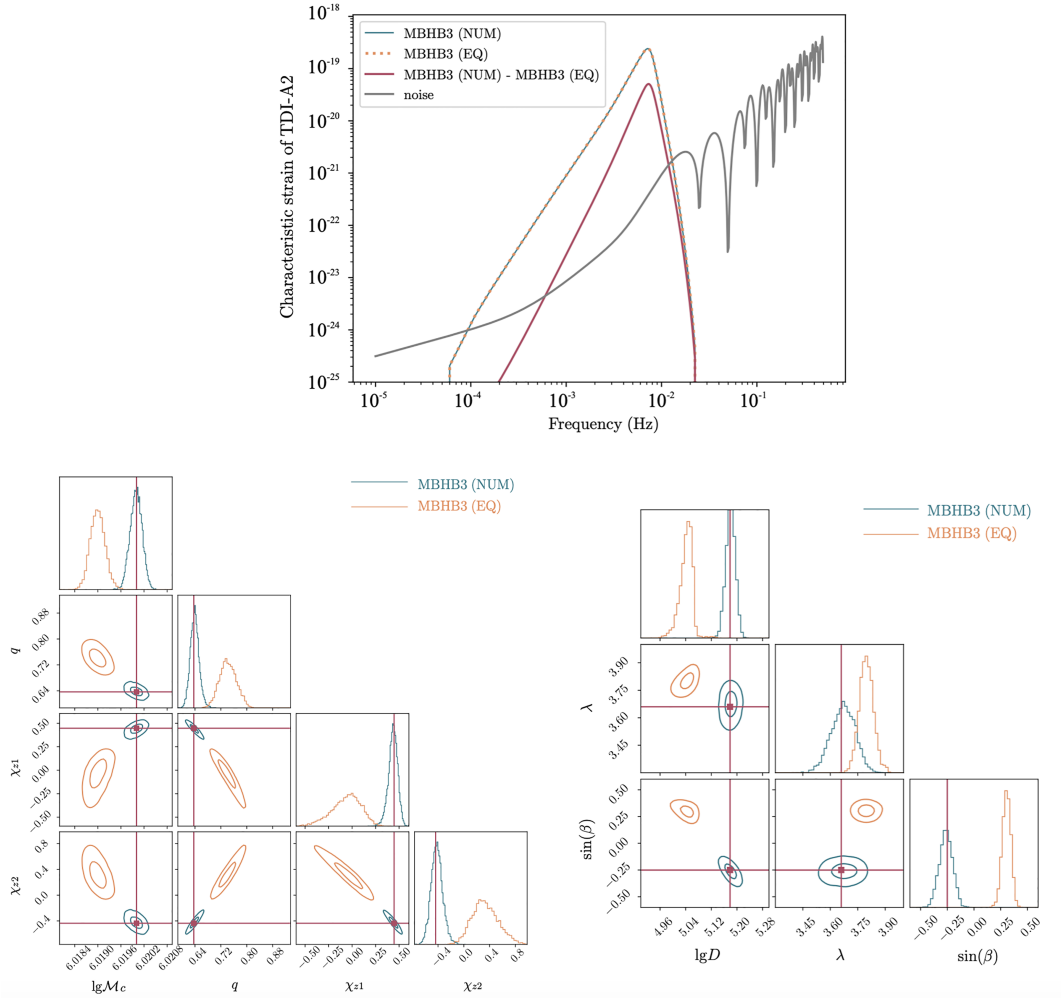

Figure 4 (Color online) Systematic errors induced by an inaccurate orbit model. Using the same source parameters as Figure 3 as an example, the data of the TDI-X_2 channel are simulated in the time domain, with GW response calculated based on a numerical orbit. Notice that we have excluded instrumental noises to isolate systematic biases from statistical uncertainties. When estimating the MBHB's source parameters, two response templates are employed: (1) faithfully adopting the same numerical orbit, and (2) using an analytical equal-arm-length approximation closest to the numerical orbit. The upper panel illustrates the discrepancy between these two templates, while comparisons on the estimates for intrinsic and extrinsic (3D localization) parameters are presented in the lower panels, respectively. Evidently, for MBHBs with SNRs exceeding 10^3, the incorporation of realistic orbital information is critical to avoid significant systematic biases.

1/SNR) [100, 101] is required. While the fast calculation of EMRI waveforms is hindered by their $O(10^3)$ to $O(10^5)$ harmonic modes. Current acceleration strategies, including semi-relativistic kludge models [102-105], GPU parallelization, and deep-learning techniques [106, 107], remain limited by incomplete incorporation of self-force corrections and post-adiabatic trajectories [108]. Additionally, parameter estimation is further complicated by multiple local maxima and significant ridges in the likelihood [109]. Driven by its prospects to probe astrophysics [110], cosmology [111], and gravity theory [112], ongoing research will keep focusing on developing fast, accurate templates and robust statistical inference frameworks [113, 114].

Additionally, GWs reaching the detectors are further influenced by both the sources' local environments and the GWs' propagation paths. Omission of these elements in the waveform models might also introduce bias in the analysis. For the former, examples include effects reviewed in ref. [115], including the relative motion of the source, the presence of a nearby massive object, and a gaseous background, etc., while the latter involves effects such as gravitational lensing [116-119]. For example, LISA is predicted to detect several multiply imaged GW signals during its mission lifetime [116], and the estimation is similar for Taiji. These phenomena also offer opportunities to probe the structures of lens objects, test galactic models, and constrain cosmic evolution history.

3.2 The challenges due to noises and anomalies

Accurate characterization of noises is crucial not only for the analysis of resolvable signals, but also for distinguishing among SGWB, confusion foreground, and instrumental noises [120-123]. However, unlike the LVK observatories, which utilize auxiliary data channels from various sensors for real-time noise monitoring, calibration, and isolation [124, 125], due to its space-based mission design, Taiji lacks equivalent diagnostic methods. Furthermore, the distinct environments of ground-based experiments and in-orbit operations suggest that the statistical properties of noise might not be completely determined prior to launch [35,126]. Figure 5 displays the TM ACC noises (left panel) and SC jitter noises (right panel) derived from a numerical simulation for the DFACS [47]. As shown, each noise component meets Taiji's design sensitivity requirements (black dashed curves), yet none of them are fully aligned with the design curves. These discrepancies, together with the signal-dominated regime, highlight the necessity of joint parameter estimation on signals and noises, using the limited data transmitted to Earth [127,128]. The agnostic of noise spectral profile requires flexible modeling as well as trans-dimensional search in unknown parameter space [35, 126, 129].

Additionally, noise characteristics also inherently depend on the TDI configurations. The widely adopted Michelson $\{A, E, T\}$ channels are usually referred to as the "optimal" TDI combinations in the literature [130]. Under the assumptions of equal arm-length and identical noise spectra for each MOSA and each laser link, the optimal combinations exhibit advantages such as noise orthogonality, which enables direct summation of the statistics (SNRs, log likelihoods, etc) across individual channels. Besides, the T channel, being insensitive to GW signals at low frequencies, can be particularly valuable as a "null" channel used for instrumental noise characterization and SGWB detection. However, for realistic orbits with unequal and time-varying arm-lengths, the optimal channels will have non-negligible noise covariance [35], thus practical data analysis must account for the covariances among channels, increasing both modeling and computational complexities. The "null" property of T channel will also be compromised at both low and high frequen-

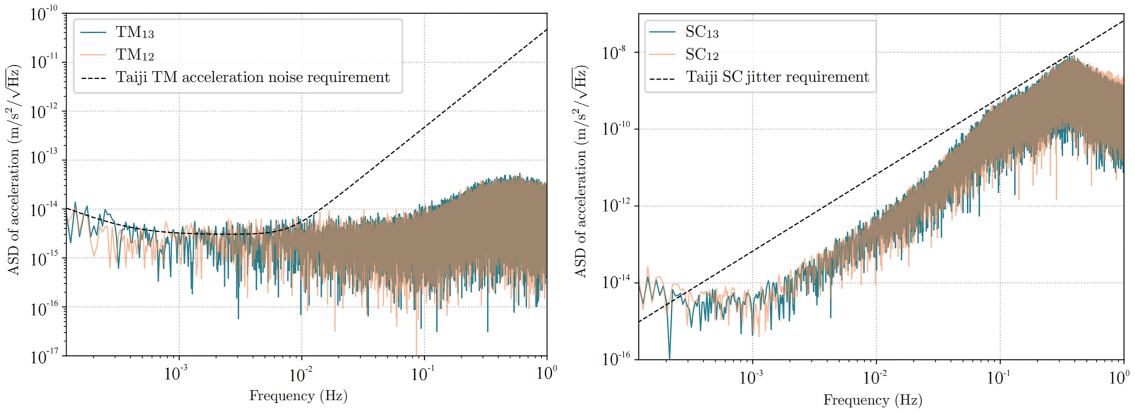

Figure 5 (Color online) The TM ACC noises (left panel) and SC jitter noises (right panel) derived from the numerical simulation for the DFACS. Each noise component meets Taiji's design sensitivity requirements (black dashed curves), yet none of them are fully aligned with the design curves.

cies [131]. Figure 6[1)] shows the sensitivity of the Michelson T_2 channel across a year, with different yellow curves representing the sensitivities on different days, compared to the "signal" channel Michelson-A_2. Consequently, the presumed optimality of $\{A, E, T\}$ demands further validation, and a systematic exploration of alternative TDI combinations remains imperative. Under different scenarios, various TDI schemes with specialized advantages have been developed, e.g., TDI channels suitable for noise characterization [132-136], robust against arm-length variation [137, 138], minimizing the loss due to data gap [139], designed to reduce specific noises [63, 64], etc.

Current studies on space-based GW data analysis usually assume Gaussian stationary noise and continuous data streams. While, practical in-orbit operations would inevitably encounter non-ideal conditions such as glitches, data gaps, and non-stationary noises. Firstly, a glitch is a representative form of non-Gaussian and transient noise. Documented in the data of GRACE [140], LISA Pathfinder [141], Taiji-1 [63], these transients are also anticipated for the future Taiji/LISA missions. Glitches could be harmful for scientific analysis by inducing false alarms [142], missed detections [143], and parameter estimation biases [34]. Secondly, the occurrences of data gaps, either scheduled ones due to maintenance or maneuvers (e.g., antenna repointing, frequency plan adjustments, PAAM rotation, etc.), or unscheduled ones due to in-orbit disruptions, are also expected [144, 145], resulting in an effective duty cycle of ~75% [146]. Data gaps could degrade scientific outcomes through breaking the coherence of long wave trains, insufficient SNR accumulation, increased noise floor caused by spectral leakage, or inducing extra uncertainty in parameter estimation [34, 147-149]. Thirdly, non-stationary noises might emerge from various mechanisms. A guaranteed contributor is the cyclostationary astrophysical foreground caused by the anisotropic distribution of GBs [120, 150]. Other mechanics include instrumental noise drifts due to the variations of payloads and SC platforms during the multi-year mission lifetimes, as evidenced in LISA Pathfinder [151-153]. This time-varying noise necessitates real-time characterization and calibration. Crucially, non-stationarity would violate the fundamental assumptions of the conventional Whittle likelihood framework [154], significantly increasing computational demands for Bayesian inference [155].

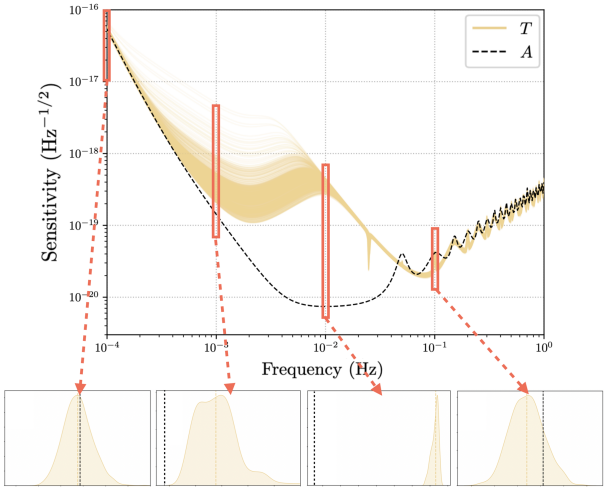

Figure 6 (Color online) The sensitivity of the Michelson-T_2 (yellow curves) channel across a year, compared to the "signal" channel Michelson-A_2 (black dashed curve). We have selected four representative frequencies, whose sensitivity distributions are displayed in the three subplots below.

3.3 The "global fit" challenge

The data of space-based GW detection is often metaphorically described as a cocktail, since it is a mixture of noises and numerous overlapping signals. The sensitive band of Taiji and LISA contains tens of millions of GW sources, each with a duration up to months or years. Therefore, signal overlapping in both the time domain and the frequency domain are ubiquitous. For data $d = n + h^{\rm true}_{\rm total} = n + \sum_i h^{\rm true}_i$, assuming that the statistical property of noise n, as well as the types and numbers of signal templates $h^{\rm tem}_i$ are known (although not in practice), the full logarithmic likelihood can be written as

$$\begin{aligned}\ln\mathcal{L} &= -\frac{1}{2}\left(d-h^{\rm tem}_{\rm total}\middle|d-h^{\rm tem}_{\rm total}\right)\\ &= -\frac{1}{2}\left(\sum_i h^{\rm tem}_i\middle|\sum_j h^{\rm tem}_j\right)+\left(\sum_i h^{\rm tem}_i\middle|d\right)+\text{const.}\\ &= -\frac{1}{2}\sum_i\left(h^{\rm tem}_i|h^{\rm tem}_i\right)+\sum_i\left(h^{\rm true}_i|h^{\rm tem}_i\right)+\sum_i\left(n|h^{\rm tem}_i\right)\\ &\quad -\sum_{i<j}\left(h^{\rm tem}_j|h^{\rm tem}_i\right)+2\sum_{i<j}\left(h^{\rm true}_j|h^{\rm tem}_i\right)+\text{const.}\\ &\neq \sum_i \ln\mathcal{L}_i,\end{aligned} \tag{7}$$

where $\mathcal{L}_i$ is the likelihood function defined by comparing the ith individual signal to corresponding template (i.e., $\ln\mathcal{L}_i \equiv -1/2(h^{\rm tem}_i|h^{\rm tem}_i) + (h^{\rm true}_i|h^{\rm tem}_i) + \text{const.}$). Namely, due to the coupling between signals, estimating all the source parameters requires simultaneous modeling of the overlapping sig-

1) In principle, PSD can effectively describe the statistical properties of noise only under the condition that the noise is Gaussian and stationary. Here, the variation of the TDI noise profile is induced by arm-length variation, which has a timescale of a month (see Figure 10). Therefore, for the observation of transient signals with durations on the order of days (such as the MBHB merger), the noise can still be treated as locally stationary. This allows for the use of PSD and the calculation of sensitivity within the relevant time intervals of interest.

nals, rather than analyzing them in an individual or sequential manner. In other words, imperfect waveform subtraction risks residual contamination and biased subsequent analyses. Meanwhile, the detectability of a signal is determined not only by its intrinsic SNR but also by the coupling with other signals. Global fitting generally involves searching $O(10^5)$ parameters across the parameter spaces of signals and noises, hence creating computational bottlenecks, given that full Bayesian analysis of a single signal using nested sampling [156] or Markov chain Monte Carlo (MCMC) [157] is already a time-consuming task. Besides, overlapping signals with similar morphologies (especially GBs) further require extra algorithms and computational powers for trans-dimensional sampling or model selection [95]. At last, except for signals, instrument noises, SGWBs, and confusion foregrounds all manifest as stochastic components of data, further complicating noise characterization and source separation.

In order to develop algorithms to resolve this mixture, efforts (e.g., refs. [32, 40-42, 127, 158, 159]) have been made on earlier mock datasets (MLDC/LDC), demonstrating that it is possible to jointly estimate the parameters of signals and noises. These prototype pipelines typically demands week(s) of computation, where the employed or developed techniques include F-statistics, parallel tempering MCMC (PTMCMC) [160], reversible jump (or trans-dimensional) MCMC [161], particle swarm optimization [162], differential evolution optimization [163], as well as fast and parallelizable (on CPU/GPU) waveform calculators [94,164-167], etc. It should be noticed that, as discussed in Section 1, these datasets were built on idealistic assumptions, including equal-arm-length analytic orbits, simplified waveform models, mildly overlapping signals, and Gaussian stationary noises with known spectral shapes. Therefore, global fit remains the core challenge for space-based GW data analysis, and current methodologies must be rigorously re-examined and extended in more realistic scenarios.

3.4 The coupling issues between pre-processing and scientific analysis

The coupling between pre-processing (noise suppression, operating parameter calibration, etc.) and scientific analysis (signal detection, source parameter estimation, etc.) arises due to their shared dependence on the interferometer readouts. The dominating bright GW signals may impede noise and instrument calibration, while imperfect noise suppression or inaccurate noise characterization in turn degrades the reliability of GW source inference based on the residual data. Under this topic, identified challenges in existing research include TDI ranging (a data-driven approach for inter-spacecraft ranging), the estimation and subtraction of TTL noises [32,168], etc. These challenges underscore the necessity of developing more comprehensive end-to-end pipeline, and demand the incorporation of all these signals, noises and instrumental effects into simulation.

4 The TDC II datasets

4.1 Data simulation pipeline

As introduced in Section 2, Taiji's data flow incorporates sophisticated in-orbit measurements and on-ground processing steps. In order to simulate the performances of instruments and the characteristics of data within a reasonable timescale, we currently focus on the key information propagating through the system, rather than implementing a full physical simulation. For Taiji's scientific data, which mainly originates from laser interferometric measurements, we outline the framework of modeling and simulation as: laser sources → laser propagation → laser interferometry → signal sampling triggered by the on-board clocks → phasemeter readout → TDI processing and scientific analysis. The simulations for GRS and DFACS constitute critical inputs to the aforementioned framework (to be detailed in separate publications). Specifically, provided by these simulations are the orbital motions of SCs, TM ACC noises, SC jitters, MOSA angular jitters, etc.

In Figure 7, the grey branch represents the simulation framework of laser interferometry measurements, with the upper red blocks denoting the physical processes and factors contributing to each stage, while the lower yellow blocks denoting the noises and GW signals newly introduced at each stage. The simulations of GRS and DFACS, as well as their outputs, are schematically shown with the blue branch. Notice that we have neglected the downsampling step (from the sampling rate of phasemeter, typically $O(10)$-$O(10^2)$ MHz [169, 170], to the sampling rate used for telemetry and data processing, $O(1)$-$O(10)$ Hz) and directly simulate at the sampling rate of the final output data. This simplification aims to avoid the computational and storage costs caused by the massive volume of raw data.

By design, the phasemeter of Taiji can output both phase and instantaneous frequency of interferometric signals [169-171]. In principle, data expressed in these two units are equivalent and can be easily transformed in to each other via differentiation or integration. Using frequency units is generally more convenient in terms of storage, telemetry, and simulation, since it remains at the same order of magnitude through the whole mission lifetime, and can be represented as double-precision floating-point numbers [172]. Therefore,

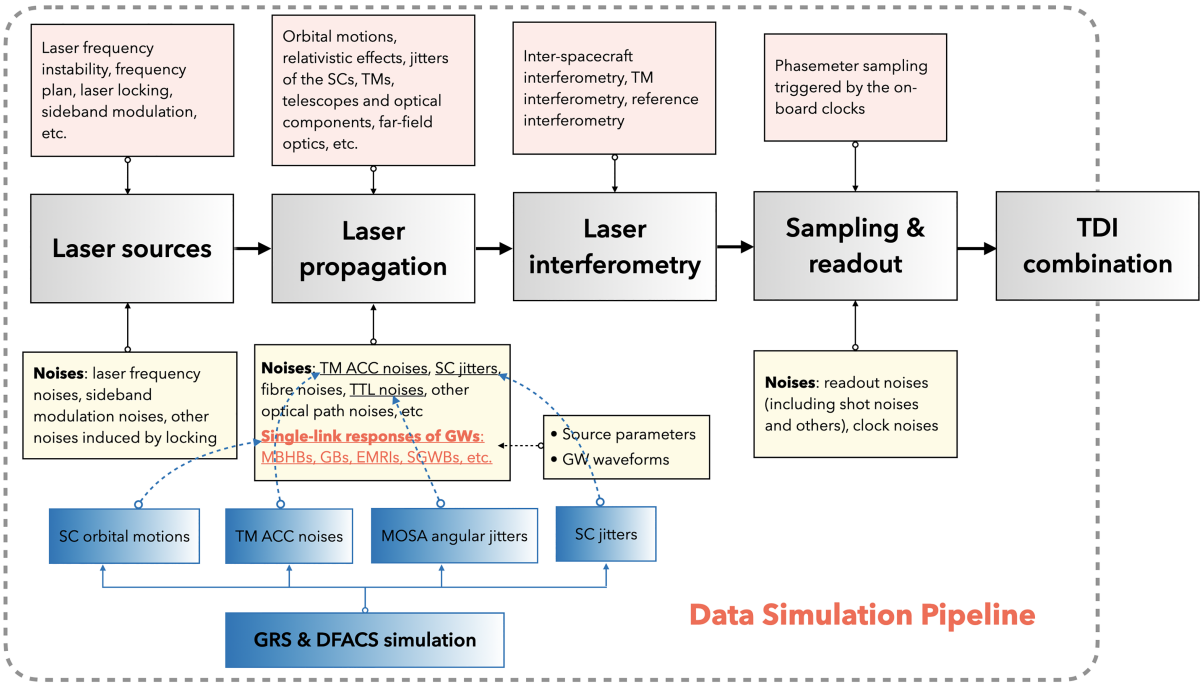

Figure 7 (Color online) A concise view of the data simulation pipeline. The grey branch represents the simulation framework of laser interferometry measurements, with the upper red blocks denoteing the physical processes and factors contributing to each stage, while the lower yellow blocks denoting the noises and GW signals newly introduced at each stage. The simulations of GRS and DFACS, as well as their outputs, are schematically shown with the blue branch (to be detailed in separate publications).

we simulate laser interferometry with frequency units, and the outputs are further converted to fractional frequency differences by dividing the central frequency of laser (281.6 THz), to align with the convention of most literature.

Within this framework, we list the models utilized in the creation of TDC II as follows (also see Figure 8 for a more brief summary). Readers may refer to *TDC II Manual* [173] for the mathematical formalism of these models, as well as their code implementations in `Triangle`.

(1) Source populations. For MBHBs, we randomly draw the source parameters from the mix of 3 population models (PopIII, Q3delay, Q3nodelay) [174], each normalized according to the predicted event rates [92]. The GB population includes 55 LISA verification Galactic binaries (VGBs) [175, 176] (or more precisely, 55 "detectable" Galactic binaries, as defined in ref. [176]), and $\sim 4.5 \times 10^7$ GBs generated from an observation-driven population model [177] adjusted for Taiji (we expanded the lower limit of GW frequency from 0.1 to 0.05 mHz due to Taiji's better sensitivity at low frequencies). To offer a preliminary estimate on the number of detectable GBs within this population and the spectral shape of confusion foreground, we employ the iterative subtraction method presented in refs. [25, 178]. Setting a widely adopted SNR threshold of 7 and observation time of 1 year, the theoretical upper limit for detectable GBs is $\sim 1.9 \times 10^4$, and the ASD of foreground is shown with black curve in Figure 9. Besides, for the 4 injected EMRI signals, typical values of the source parameters are adopted.

(2) Waveforms. For MBHBs, three different approximants are adopted for different challenge topics: IMRPhenomD [179, 180], IMRPhenomT [180-182], and SEOBNRv5EHM [183, 184]. As for GBs, we adopt the waveform under Newtonian approximation and expand the phase evolution up to the second derivative of GW frequency. The injected EMRI waveforms include the augmented kludge (AK) model [105], the EMRI waveforms of Kerr black hole (BH) and Bumpy BH [185, 186], as well as the b-EMRI waveform, which is the EMRI system produced by tidal capture of binary black holes [187, 188]. Besides, we model the astrophysical origin SGWB with a power-law spectrum, and cosmological SGWB (first-order phase transition) with a double broken power-law spectrum [127]. The detector responses are calculated in time-domain response based on the rigorous formalism known so far [38, 94, 189] (i.e., no equal-arm-length or low-frequency or static constellation approximations).

(3) Orbit. The dynamics of SCs serve as critical inputs for both GW response calculation and noise simulation. The numerical orbit utilized in TDC II is derived from a 60-degree-of-freedom simulation for DFACS, performed by the Innovation Academy for Microsatellites of CAS [47]. The simulation is conducted with quadruple-precision floating-point

Figure 8 (Color online) The models behind TDC II.

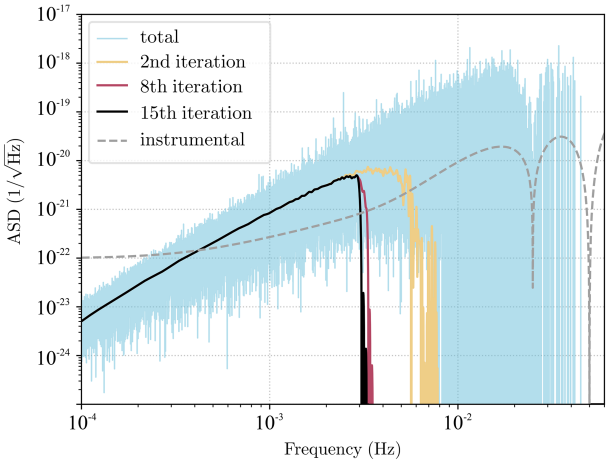

Figure 9 (Color online) Preliminary estimation for the shape of the confusion foreground. The calculation is based on an SNR threshold of 7 and a 1-year observation time (in consistence with the datasets). We run the subtraction algorithm [25, 178] for 15 iterations to ensure convergence.

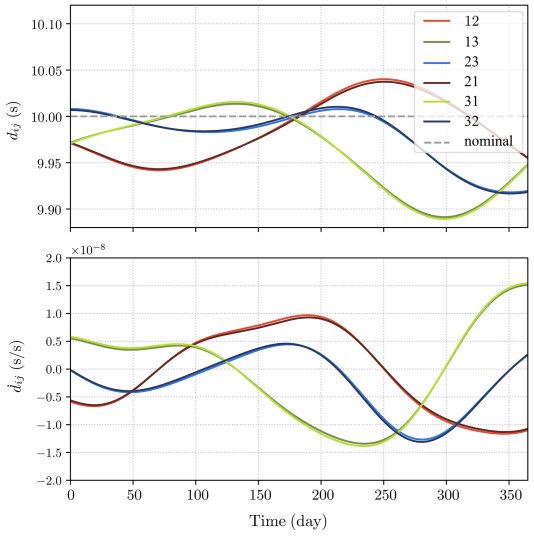

Figure 10 (Color online) The light travel times (upper panel) and their derivatives (lower panel) along 6 arms $ij \in \{12, 23, 31, 21, 32, 13\}$ calculated according to the simulated Taiji orbit. The grey dashed line represents the nominal arm-length (10 s, i.e., 3×10^9 m) of Taiji. During the mission time of one year, the orbit has a maximum arm-length difference of $O(1\%)$ and a maximum arm-length variation rate of less than 5 m/s.

numbers and incorporates the effects of gravitational perturbations from celestial bodies, the forces acted by micro-thrusters, and solar radiation pressure, etc. As can be seen in Figure 10, during the mission time of 1 year, the orbit has a maximum arm-length difference of $O(1\%)$ and maximum arm-length variation rate of less than 5 m/s, fully compliant with Taiji's design requirements [12, 190].

(4) Noises. The noise data of TDC II originate from two

distinct sources: those related to the motions of SCs and TMs are extracted from GRS & DFACS simulation, including the ACC noise of TMs, the jitters of SCs, and the angular jitters of MOSAs (used to further simulate the inter-spacecraft TTL noise via a simple linear coupling model [61]), etc.; while others are generated according to Taiji's design noise curves, e.g., the readout noises of interferometers. Additionally, glitches are simulated with the LISA Pathfinder legacy model [141, 191].

4.2 The TDC II datasets

The current release of TDC II comprises 5 groups of datasets (Figure 11), each targeting specific challenge topics listed in Section 3. Except for group 0, designed as illustrative examples for the access and use of TDC II, most of the remaining datasets are blind (i.e., the source parameters are unknown).

Groups 1 and 2 focus on building the tools for scientific analysis. These data are presented in the form of single-link

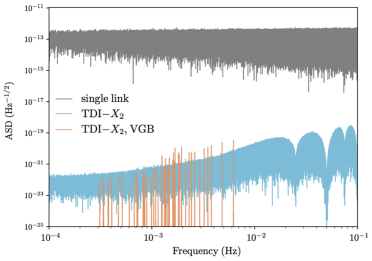

TDC II-0.1: VGBs (ASD).

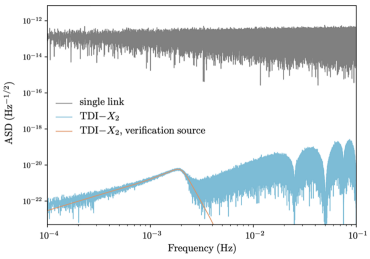

TDC II-0.2: single MBHB (ASD).

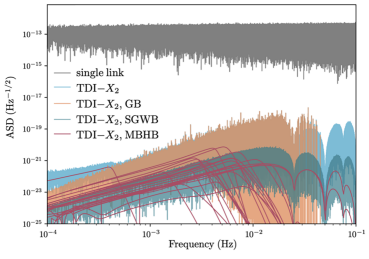

TDC II-1.1: multi-source (ASD).

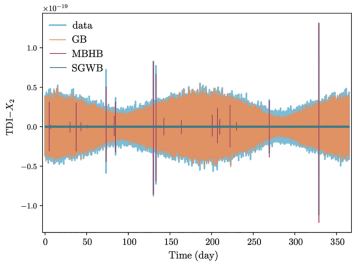

TDC II-1.1: multi-source (time series, downsampled to 0.1 Hz).

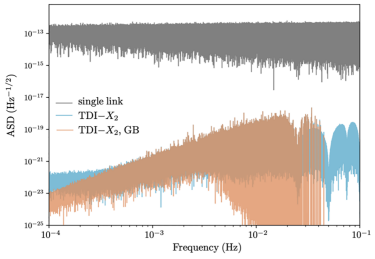

TDC II-2.1: GBs (ASD).

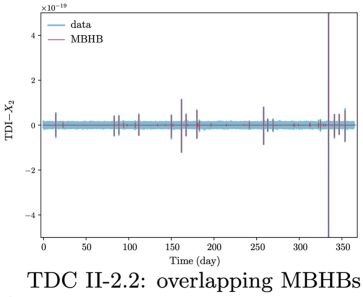

TDC II-2.2: overlapping MBHBs (time-series, downsampled to 0.1 Hz).

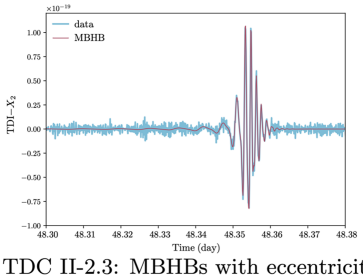

TDC II-2.3: MBHBs with eccentricity and higher harmonics (time-series, downsampled to 0.1 Hz, zoomed in around one of the mergers).

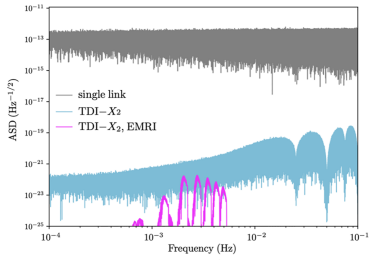

TDC II-2.5: EMRI (ASD, one of the four EMRIs is shown as a representative case).

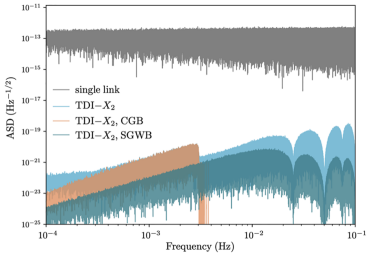

TDC II-2.8: SGWB (ASD).

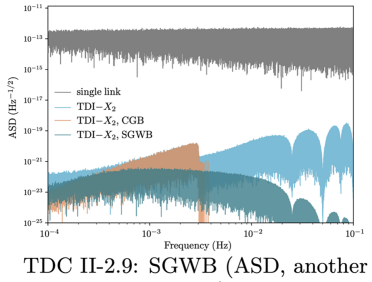

TDC II-2.9: SGWB (ASD, another profile).

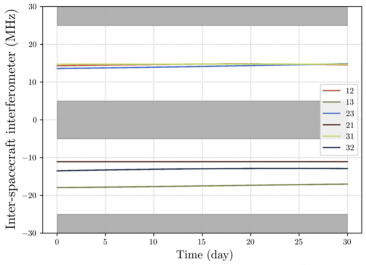

TDC II-3.1: raw ISI readouts (time series).

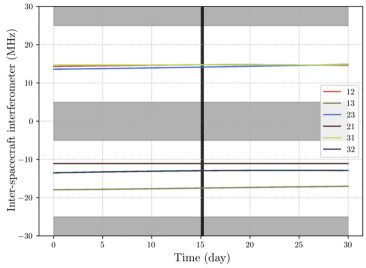

TDC II-4.1: raw ISI readouts (time series, gap shown as a black vertical line).

Figure 11 (Color online) The TDC II datasets, either shown in the time domain or frequency domain (as ASDs) for optimal visualization.

measurements η_{ij} (in the fractional frequency difference unit, see eq. (2) for definition), instead of the $\{X, Y, Z\}$ or $\{A, E, T\}$ TDI combinations. One may notice that this is a significant change relative to the previous data challenges [36-38], motivated by the need to systematically investigate the performances of diverse TDI configurations on GW detection, noise suppression, and characterization, etc. (see Sections 3.1 and 3.2). Users may construct customized TDI variables utilizing the tools and examples provided by the `Triangle` code. The injected laser frequency noise offers an intrinsic metric to validate the basic functionality of TDI schemes. Besides, the sampling rate is set to 1 Hz (although the raw sampling rate of telemetry data is higher than 1 Hz, it should suffice for GW signals), and all the data have been perfectly detrended and synchronized to TCB. The injected noise types include laser frequency noise, TM ACC noise, readout noises of interferometers (ISIs, RFIs, TMIs), optical path noises, and fibre back link noise.

Groups 3 and 4 are designed to establish an end-to-end data analysis pipeline, therefore these two sets are presented in the form of raw laser interferometric measurements in the frequency (Hz) unit, namely the readouts of ISIs, RFIs, and TMIs, each including a carrier and a sideband measurement, together with the auxiliary data (pseudo ranges, angular jitters read by the differential wavefront sensors, orbit determination, measured clock deviations from TCB). These data are recorded according to the on-board clocks, which deviate from TCB due to instrumental imperfections and relativistic corrections. The sampling rate is set to 4 Hz. Beyond the noise components in groups 1 and 2, also incorporated in groups 3 and 4 are the clock noise, sideband modulation noise, SC jitter, TTL noise, as well as the readout noises of auxiliary data.

Despite the anticipated mission lifetime of at least five years, the maximum duration of the mock data is one year. This is primarily limited by the computational cost of spacecraft dynamics simulation. Due to the need to solve high-dimensional differential equations with quadruple-precision numbers, the generation of one-year orbital data typically takes several weeks. However, considering the realistic scenario of future detection, we believe that the current duration of mock data remains viable for algorithm development and GW scientific research. For future space-based detection, to ensure the timeliness of scientific outputs, global analysis may be conducted weekly or monthly as new data arrive, rather than after the whole mission lifetime. Therefore, simulated data spanning up to five years or longer is not always necessary. Additionally, we also plan to incorporate longer-duration mock data into TDC II in subsequent updates.

Each dataset is stored in a separate HDF5 (`.h5`) file, whose download link can be found on the website of TDC II [43]. Within the HDF5 files, all the data are organized under the attribute "`eta`" (for groups 0, 1, and 2) or attributes "`interspacecraft_interferometer_carrier`", etc (for groups 3 and 4), with the corresponding sampling times stored under "`time`". Except for these common features, in the following, we present a detailed description of each of the datasets of TDC II.

The "verification" datasets In dataset 0.0/0.1, we inject 55 VGBs/1 MBHB (IMRPhenomD waveform) upon the instrumental noises, respectively. Designed as simple datasets for illustration and validation, all the source parameters can be found in the data files. The accompanying tutorials in the `Triangle-GB` and `Triangle-BBH` codes will demonstrate a simple workflow from loading data, TDI combination, waveform modeling, to full Bayesian posterior estimation.

The "global fit" dataset The multi-source dataset of TDC II includes $\sim 4.5 \times 10^7$ GBs, 25 MBHBs, SGWB, and instrumental noises. Leveraging the well-validated signal models in the former datasets, users may concentrate on exploring and developing global analysis techniques for realistic scenarios: numerical orbit, diverse (2nd-generation) TDI configurations, unknown spectral shapes of noise and SGWB, as well as a higher level of signal overlapping (compared to LDC 2a and TDC I), etc.

The "single source" datasets Datasets in this group are tailored to address the analysis of specific signal types, including:

(1) The global analysis of GBs (dataset 2.1);

(2) The estimation of more overlapping MBHBs (dataset 2.2, 50 MBHBs/year, the IMRPhenomT waveform is utilized since it might be suitable for time-domain analysis [181]) or individual MBHBs with complex waveforms (dataset 2.3, 3 MBHBs in total, SEOBNRv5EHM waveform);

(3) The estimation of EMRI with AK, Kerr-BH, Bumpy-BH, and b-EMRI waveforms (datasets 2.4, 2.5, 2.6, 2.7, notice that, considering the widely recognized difficulty in EMRI estimation, the prior range of 2.4, as well as the parameters of more complex 2.5, 2.6, 2.7, will be provided in the data files, in order to support targeted search);

(4) the detection and discrimination of SGWBs from confusion foreground and instrumental noises (datasets 2.7, 2.8).

The "end-to-end" dataset This dataset differs from the former ones by providing raw interferometric measurements (ISIs, TMIs, RFIs) alongside auxiliary data, with extended noise types and the effect of onboard clock drift incorporated. The TCB timestamps of data and the delay times used in the TDI combination are not directly provided but must be derived through pre-processing (clock synchronization and inter-spacecraft ranging) instead. After these, the noise floor of data can be further suppressed through the subtraction of inter-spacecraft TTL noise, which is generated with a simple

linear coupling model [61]. The injected GW signals comprise a few MBHBs and GBs. This dataset aims to assist in developing an end-to-end pipeline from raw data to scientific products, and addressing the coupling issues between pre-processing and scientific analysis (e.g., TTL coefficient calibration, TDI ranging).

The "up-to-date" dataset To demonstrate the Taiji simulation group's progress in data simulation and illustrate up-to-date knowledge on realistic data, a rolling updating dataset is also created. In its initial release, this dataset is built upon the settings of the "end-to-end" dataset, with more GW signals injected, and data anomalies such as glitches and gaps are also incorporated.

It should be emphasized that the current version of TDC II should be regarded as representative, rather than an exhaustive collection of all the scientific objectives and challenging issues. Users are encouraged to go beyond the default TDC II datasets by injecting custom signals and noises using the `Triangle` toolkit, thereby broadening the scope of exploration. We also plan to continuously update TDC II in the future (e.g., by extending the duration of mock data, and injecting sBHB signals, which represent an important target for Taiji that was not included in the initial release).

The timeline for TDC II is as follows. The official release is scheduled for May 28, 2025. Prior to the official release, a beta test release will be deployed on May 23, 2025. During this period, users are encouraged to propose suggestions regarding the optimization of datasets. The first collection of TDC II results is planned on October 9, 2025, and the collected results will be summarized and made public on the website. The first dataset update will follow thereafter.

5 The TDC II toolkit: `Triangle`

The TDC II toolkit, consisting of three code repositories prefixed with "`Triangle`", is also released alongside the mock data. Within this suite, `Triangle-Simulator` is a time-domain prototype simulator for the data of space-based GW detectors. Given the models in Section 4.1 and under the settings of Section 4.2, this simulator enables full reproducibility of the TDC II data. It is designed to assist users in understanding the characteristics of Taiji data, creating their own mock data by injecting customized noises and GW waveforms, hence uncovering new data analysis challenges and scientific objectives. Furthermore, the models and functions within `Triangle-Simulator`, especially the ones related to GW responses, provide benchmarks for developing and validating data analysis tools. This simulator encapsulates the simulation of GW responses, noises, instrumental effects (e.g., clock deviations), TDI, and other pre-processing steps in a unified pipeline. Based on a modular design, it supports user-defined models (or data) for orbits, noises, and signals. In principle, `Triangle-Simulator` is generically applicable to any space-based GW detection mission with a triangular configuration, not specifically Taiji, but also missions such as LISA and TianQin. Beyond the source codes, the repository also offers 5 tutorials, covering the introductions on laser interferometric measurements, noise types and transfer functions, GW response formalism, and TDI combinations, followed by basic instructions on the access and usage of TDC II data.

The other two supplementary repositories are designed to provide illustrative examples for users (particularly students), showcasing how to perform simple Bayesian analysis on some easy tasks. They are mainly based on two frequency-domain fast signal response calculators: `Triangle-BBH` targeting MBHBs and `Triangle-GB` specialized for GBs. Under identical configurations (orbit, waveform approximants, source parameters, etc.), the frequency-domain responses are consistent with the time-domain simulations of `Triangle-Simulator`. More specifically, `Triangle-BBH` models the 2nd-generation TDI responses of MBHBs in the frequency domain, utilizing two implementations of the IMRPhenomD/HM approximants: one is CPU-based `WF4PY` [192-194], and the other is GPU-accelerated `BBHx` [164, 165, 195]. The interface for numerical orbit is the same as `Triangle-Simulator`. The speed of `Triangle-BBH` is generally 0.1-1 ms per waveform evaluation (depending on the length of frequency series and the capability of hardware), which enables Bayesian parameter estimation of MBHBs. On the other hand, `Triangle-GB` calculates the 2nd-generation TDI responses of GBs, which is adapted from `GBGPU` [166, 167, 196] (the GPU implementation of `FastGB` algorithm [95]) in order to support the numerical orbit of Taiji and 2nd-generation TDI combinations. The speed is up to 10 to 100 μs per GB waveform. Examples for the analysis of TDC "verification" datasets 0.1 and 0.2 are offered in these repositories, with one of them based on `Triangle-GB` shown in Appendix. One should notice that these examples should only be seen as illustrative, but not as solutions to all the challenges.

6 Summary and outlook

In this paper, we systematically reviewed the anticipated data analysis challenges for the realistic observation of Taiji, and introduced a new simulation testbed for data analysis, including TDC II, a collection of mock datasets intended to support the research towards addressing these challenges, and an open-source toolkit `Triangle`. Collectively, they will as-

sist in the development of Taiji's data analysis tools in the upcoming stage.

In the future, the Taiji simulation group will continue enhancing the realism and reliability of mock data by incorporating more physical models for the GRSs, the far-field optics (especially the wavefront errors caused by telescope aberrations and their far-field propagation) [197], the impacts of thermal stability on core metrology systems, the effects of stray lights [198], the onboard optical delays [199], the effects of digitization and downsampling filters [200,201], etc., and further integrate the readouts of auxiliary sensors to support the development of more "end-to-end" pipelines. Especially, keen attention will be paid to the models that have been validated via ground-based experiments. Besides, the GW source catalogs and waveforms will also be continuously updated, in alignment with the frontier developments in astronomy and cosmology.

Looking ahead, joint space-based detection with future LISA-Taiji or LISA-Taiji-TianQin networks [15, 73-75] could enhance the detectability of GW signals, hence enabling unprecedented tests of astrophysics, cosmology, and fundamental physics. Therefore, future TDC should also expand its scope to include other detectors. Researchers would have the opportunity to leverage cross-mission data to refine noise calibration and mitigation, improve source localization, and most importantly, perform high-confidence detection of SGWBs.

The development of TDC II was supported by the National Key Research and Development Program of China (Grant Nos. 2024YFC2207300, 2021YFC2201903, 2021YFC2201901, 2020YFC2200100). The creation of mock data significantly depends on the DFACS simulation conducted by the Innovation Academy for Microsatellites of CAS. We acknowledge the contributions of National Space Science Center of CAS, Shanghai Astronomical Observatory of CAS, and Peking University for providing essential noise models, GW waveform data and GW source catalogs. Collaborative support was also offered by the University of Chinese Academy of Sciences, Beijing Normal University, as well as other institutes, groups and individuals. Also, we are grateful for the anonymous reviewers' comments and suggestions during the review process. For the use of `Triangle` *in your published research works, please cite the references provided in the README files.*

Conflict of interest The authors declare that they have no conflict of interest.

1 J. Aasi, B. P. Abbott, R. Abbott, T. Abbott, M. R. Abernathy, K. Ackley, C. Adams, T. Adams, P. Addesso, R. X. Adhikari, et al., Class. Quantum Grav. **32**, 074001 (2015).
2 F. Acernese, M. Agathos, K. Agatsuma, D. Aisa, N. Allemandou, A. Allocca, J. Amarni, P. Astone, G. Balestri, G. Ballardin, et al., Class. Quantum Grav. **32**, 024001 (2014).
3 T. Akutsu, M. Ando, K. Arai, Y. Arai, S. Araki, A. Araya, N. Aritomi, Y. Aso, S. Bae, Y. Bae, et al., Prog. Theor. Exp. Phys. **2021**, 101 (2021).
4 G. Agazie, A. Anumarlapudi, A. M. Archibald, Z. Arzoumanian, P. T. Baker, B. Bécsy, L. Blecha, A. Brazier, P. R. Brook, S. Burke-Spolaor, et al., Astrophys. J. Lett. **951**, L8 (2023).
5 J. Antoniadis, S. Babak, A. S. Bak Nielsen, C. G. Bassa, A. Berthereau, M. Bonetti, E. Bortolas, P. R. Brook, M. Burgay, R. N. Caballero, et al., Astron. Astrophys. **678**, A48 (2023).
6 D. J. Reardon, A. Zic, R. M. Shannon, G. B. Hobbs, M. Bailes, V. Di Marco, A. Kapur, A. F. Rogers, E. Thrane, J. Askew, et al., Astrophys. J. Lett. **951**, L6 (2023).
7 H. Xu, S. Chen, Y. Guo, J. Jiang, B. Wang, J. Xu, Z. Xue, R. Nicolas Caballero, J. Yuan, Y. Xu, et al., Res. Astron. Astrophys. **23**, 075024 (2023).
8 P. Amaro-Seoane, H. Audley, S. Babak, J. Baker, E. Barausse, P. Bender, E. Berti, P. Binetruy, M. Born, D. Bortoluzzi, et al., arXiv: 1702.00786.
9 J. Baker, J. Bellovary, P. L. Bender, E. Berti, R. Caldwell, J. Camp, J. W. Conklin, N. Cornish, C. Cutler, R. DeRosa, et al., arXiv: 1907.06482.
10 W. R. Hu, and Y. L. Wu, Natl. Sci. Rev. **4**, 685 (2017).
11 Z. Luo, Z. K. Guo, G. Jin, Y. Wu, and W. Hu, Results Phys. **16**, 102918 (2020).
12 Z. Luo, Y. Wang, Y. Wu, W. Hu, and G. Jin, Prog. Theor. Exp. Phys. **2021**, 108 (2021).
13 J. Luo, L. S. Chen, H. Z. Duan, Y. G. Gong, S. Hu, J. Ji, Q. Liu, J. Mei, V. Milyukov, M. Sazhin, et al., Class. Quantum Grav. **33**, 035010 (2016).
14 Y. Gong, J. Luo, and B. Wang, Nat. Astron. **5**, 881 (2021).
15 R. G. Cai, Z. K. Guo, B. Hu, C. Liu, Y. Lu, W. T. Ni, W. H. Ruan, N. Seto, G. Wang, and Y. L. Wu, Fundamental Res. **4**, 1072 (2024).
16 European Space Agency, Capturing the ripples of spacetime: LISA gets go-ahead, 2024, https://www.esa.int/Science_Exploration/Space_Science/LISA/Capturing_the_ripples_of_spacetime_LISA_gets_go-ahead.
17 Y. L. Wu, Z. R. Luo, J. Y. Wang, M. Bai, W. Bian, H. W. Cai, R. G. Cai, Z. M. Cai, J. Cao, B. Chen, et al., Int. J. Mod. Phys. A **36**, 2102002 (2021).
18 H. S. Liu, Z. R. Luo, and W. Sha, Int. J. Mod. Phys. A **36**, 2140004 (2021).
19 Z. Wang, and J. G. Lei, Int. J. Mod. Phys. A **36**, 2140008 (2021).
20 S. Y. Xu, L. X. Xu, L. X. Cong, Y. G. Li, and C. F. Qiao, Int. J. Mod. Phys. A **36**, 2140013 (2021).
21 Z. Hu, P. Wang, J. Deng, Z. Cai, Z. Wang, Z. Wang, J. Yu, Y. Wu, Q. Kang, H. Li, et al., Int. J. Mod. Phys. A **36**, 2140019 (2021).
22 X. Peng, H. Jin, P. Xu, Z. Wang, Z. Luo, X. Ma, L. E. Qiang, W. Tang, X. Ma, Y. Zhang, et al., Int. J. Mod. Phys. A **36**, 2140026 (2021).
23 H. Zhang, P. Xu, Z. Ye, D. Ye, L. E. Qiang, Z. Luo, K. Qi, S. Wang, Z. Cai, Z. Wang, et al., Remote Sens. **15**, 3817 (2023).
24 L. Wu, P. Xu, S. Zhao, L. E. Qiang, Z. Luo, and Y. Wu, Microgravity Sci. Technol. **34**, 77 (2022).
25 C. Liu, W. H. Ruan, and Z. K. Guo, Phys. Rev. D **107**, 064021 (2023).
26 Z. W. Zhao, L. F. Wang, J. F. Zhang, and X. Zhang, Sci. Bull. **65**, 1340 (2020).
27 L. F. Wang, S. J. Jin, J. F. Zhang, and X. Zhang, Sci. China-Phys. Mech. Astron. **65**, 210411 (2022).
28 J. R. Gair, L. Barack, T. Creighton, C. Cutler, S. L. Larson, E. S. Phinney, and M. Vallisneri, Class. Quantum Grav. **21**, S1595 (2004).
29 J. Chen, C. S. Yan, Y. J. Lu, Y. T. Zhao, and J. Q. Ge, Res. Astron. Astrophys. **21**, 285 (2021).
30 B. R. Wang, and J. Li, Phys. Rev. D **109**, 063520 (2024).
31 Z. C. Chen, and L. Liu, Eur. Phys. J. C **84**, 1176 (2024).
32 T. B. Littenberg, and N. J. Cornish, Phys. Rev. D **107**, 063004 (2023).
33 N. Afshordi, S. Akay, P. Amaro-Seoane, A. Antonelli, J. C. Aurrekoetxea, L. Barack, E. Barausse, R. Benkel, L. Bernard, S. Bernuzzi, et al., arXiv: 2311.01300.
34 E. Castelli, Q. Baghi, J. G. Baker, J. Slutsky, J. Bobin, N. Karnesis, A. Petiteau, O. Sauter, P. Wass, and W. J. Weber, Class. Quantum Grav. **42**, 065018 (2025).
35 Q. Baghi, N. Karnesis, J. B. Bayle, M. Besançon, and H. Inchauspé,

J. Cosmol. Astropart. Phys. **2023**, 066 (2023).
36 K. A. Arnaud, S. Babak, J. G. Baker, M. J. Benacquista, N. J. Cornish, C. Cutler, S. L. Larson, B. S. Sathyaprakash, M. Vallisneri, A. Vecchio, et al., AIP Conf. Proc. **873**, 619 (2006).
37 Q. Baghi, arXiv: 2204.12142.
38 Z. Ren, T. Zhao, Z. Cao, Z. K. Guo, W. B. Han, H. B. Jin, and Y. L. Wu, Front. Phys. **18**, 64302 (2023).
39 E. K. Li, H. Wang, H. Y. Chen, H. Fan, Y. N. Li, Z. Y. Li, Z. C. Liang, X. Y. Lyu, T. X. Wang, Z. Wu, et al., Class. Quantum Grav. **42**, 165005 (2025).
40 S. H. Strub, L. Ferraioli, C. Schmelzbach, S. C. Stähler, and D. Giardini, Phys. Rev. D **110**, 024005 (2024).
41 M. L. Katz, N. Karnesis, N. Korsakova, J. R. Gair, and N. Stergioulas, arXiv:2405.04690
42 S. Deng, S. Babak, M. Le Jeune, S. Marsat, É. Plagnol, and A. Sartirana, Phys. Rev. D **111**, 103014 (2025).
43 Taiji Laboratory for Gravitational Wave Universe, Taiji Data Challenge II Website, 2025, http://gr.imech.ac.cn/overview.
44 J. Wang, K. Q. Qi, S. X. Wang, R. H. Gao, P. Li, R. Yang, H. S. Liu, and Z. R. Luo, Sci. Sin.-Phys. Mech. Astron. **54**, 270405 (2024).
45 H.-S. Liu, R.-H. Gao, Z.-R. Luo, and G. Jin, Chin. Optics **12**, 486 (2019).
46 R.-J. Deng, Y.-B. Zhang, H.-S. Liu, and Z.-R. Luo, Chin. Optics **16**, 765 (2023).
47 Q. Xu, B. Cui, P. Wang, Y. Xia, and Y. Zhang, Chin. J. Space Sci. **44**, 903 (2024).
48 J. N. Reinhardt, M. Staab, K. Yamamoto, J. B. Bayle, A. Hees, O. Hartwig, K. Wiesner, S. Shah, and G. Heinzel, Phys. Rev. D **109**, 022004 (2024).
49 M. Du, P. Wu, Z. Luo, and P. Xu, Results Phys. **62**, 107819 (2024).
50 Y. Wang, G. Heinzel, and K. Danzmann, Phys. Rev. D **90**, 064016 (2014).
51 J. Niklas Reinhardt, O. Hartwig, and G. Heinzel, Class. Quantum Grav. **42**, 055014 (2025).
52 W.-T. Ni, J.-T. Shy, S.-M. Tseng, X. Xu, H.-C. Yeh, W.-Y. Hsu, W.-L. Liu, S.-D. Tzeng, P. Fridelance, E. Samain, et al., in *Progress in mission concept study and laboratory development for the astrodynamical space test of relativity using optical devices(ASTROD)*: *Proceedings of Spacecraft, Space Environments, and Instrumentation Technologies*. San Diego, SIPE, 1997.
53 J. W. Armstrong, F. B. Estabrook, and M. Tinto, Astrophys. J. **527**, 814 (1999).
54 M. Tinto, and S. V. Dhurandhar, Living Rev. Relativ. **24**, 1 (2021).
55 O. Hartwig, J. B. Bayle, M. Staab, A. Hees, M. Lilley, and P. Wolf, Phys. Rev. D **105**, 122008 (2022).
56 G. Wang, W. T. Ni, W. B. Han, and C. F. Qiao, Phys. Rev. D **103**, 122006 (2021).
57 M. Otto, G. Heinzel, and K. Danzmann, Class. Quantum Grav. **29**, 205003 (2012).
58 M. Tinto, and O. Hartwig, Phys. Rev. D **98**, 042003 (2018).
59 O. Hartwig, and J. B. Bayle, Phys. Rev. D **103**, 123027 (2021).
60 Q. Jiang, P. Dong, H.-S. Liu, Z.-Ren. Luo, Chin. Optics **16**, 1394 (2023).
61 S. Paczkowski, R. Giusteri, M. Hewitson, N. Karnesis, E. D. Fitzsimons, G. Wanner, and G. Heinzel, Phys. Rev. D **106**, 042005 (2022).
62 X. Wang, J. Yang, Z. Cui, Y. Wang, J. Jia, and L. Zhang, Phys. Rev. D **110**, 102004 (2024).
63 P. Wu, M. Du, and P. Xu, Opt. Express **32**, 43249 (2024).
64 Y. J. Tan, W. S. Huang, P. P. Wang, Z. Q. Wu, J. M. Le Floch, H. Z. Wu, J. Liu, C. G. Shao, and Z. B. Zhou, Phys. Rev. D **111**, 024011 (2025).
65 X. Wei, L. Huang, T. Shen, Z. Cai, and J. He, Phys. Rev. D **108**, 082001 (2023).
66 M. Otto, *Time-Delay Interferometry Simulations for the Laser Interferometer Space Antenna*. Dissertation for the Doctoral Degree (Gottfried Wilhelm Leibniz Universität, Hannover, 2016).
67 O. Hartwig, *Instrumental Modelling and Noise Reduction Algorithms for the Laser Interferometer Space Antenna*. Dissertation for the Doctoral Degree (Gottfried Wilhelm Leibniz Universität, Hannover, 2021).
68 N. J. Cornish, Phys. Rev. D **105**, 044007 (2022).
69 H. Y. Chen, X. Y. Lyu, E. K. Li, and Y. M. Hu, Sci. China-Phys. Mech. Astron. **67**, 279512 (2024).
70 M. Du, B. Liang, H. Wang, P. Xu, Z. Luo, and Y. Wu, Sci. China-Phys. Mech. Astron. **67**, 230412 (2024).
71 B. Liang, M. Du, H. Wang, Y. Xu, C. Liu, X. Wei, P. Xu, L. Qiang, and Z. Luo, Mach. Learn.-Sci. Technol. **5**, 045040 (2024).
72 Y. Xu, H. Wang, M. Du, B. Liang, and P. Xu, Phys. Rev. D **111**, 063037 (2025).
73 W. H. Ruan, C. Liu, Z. K. Guo, Y. L. Wu, and R. G. Cai, Nat. Astron. **4**, 108 (2020).
74 G. Wang, W. T. Ni, W. B. Han, P. Xu, and Z. Luo, Phys. Rev. D **104**, 024012 (2021).
75 S. J. Jin, Y. Z. Zhang, J. Y. Song, J. F. Zhang, and X. Zhang, Sci. China-Phys. Mech. Astron. **67**, 220412 (2024).
76 A. D. Johnson, J. Roulet, K. Chatziioannou, M. Vallisneri, C. G. Trejo, and K. A. Gersbach, Phys. Rev. D **112**, 024045 (2025).
77 M. H. A. Davis, A Review of the Statistical Theory of Signal Detection, edited by B. F. Schutz, *Gravitational Wave Data Analysis* (Springer, Dordrecht, 1989).
78 P. Jaranowski, and A. Krolak, *Analysis of Gravitational-Wave Data* (Cambridge University Press, London, 2009).
79 A. J. K. Chua, and M. Vallisneri, Phys. Rev. Lett. **124**, 041102 (2020).
80 M. Dax, S. R. Green, J. Gair, J. H. Macke, A. Buonanno, and B. Schölkopf, Phys. Rev. Lett. **127**, 241103 (2021).
81 K. Chatziioannou, A. Klein, N. Yunes, and N. Cornish, Phys. Rev. D **95**, 104004 (2017).
82 V. Kapil, L. Reali, R. Cotesta, and E. Berti, Phys. Rev. D **109**, 104043 (2024).
83 L. Lindblom, B. J. Owen, and D. A. Brown, Phys. Rev. D **78**, 124020 (2008).
84 M. Pürrer, and C. J. Haster, Phys. Rev. Res. **2**, 023151 (2020).
85 C. Cutler, and M. Vallisneri, Phys. Rev. D **76**, 104018 (2007).
86 M. Garg, S. Tiwari, A. Derdzinski, J. G. Baker, S. Marsat, and L. Mayer, Mon. Not. R. Astron. Soc. **528**, 4176 (2023).
87 C. Pitte, Q. Baghi, S. Marsat, M. Besançon, and A. Petiteau, Phys. Rev. D **108**, 044053 (2023).
88 Y. Gong, Z. Cao, J. Zhao, and L. Shao, Phys. Rev. D **108**, 064046 (2023).
89 G. Pratten, P. Schmidt, H. Middleton, and A. Vecchio, Phys. Rev. D **108**, 124045 (2023).
90 C. J. Moore, E. Finch, A. Klein, V. Korol, N. Pham, and D. Robins, Mon. Not. R. Astron. Soc. **531**, 2817 (2024).
91 J. D. Liu, W. B. Han, Q. Yun, and S. C. Yang, Mon. Not. R. Astron. Soc. **532**, 4722 (2024).
92 A. Mangiagli, C. Caprini, M. Volonteri, S. Marsat, S. Vergani, N. Tamanini, and H. Inchauspé, Phys. Rev. D **106**, 103017 (2022).
93 S. Marsat, J. G. Baker, and T. D. Canton, Phys. Rev. D **103**, 083011 (2021).
94 M. L. Katz, J. B. Bayle, A. J. K. Chua, and M. Vallisneri, Phys. Rev. D **106**, 103001 (2022).
95 N. J. Cornish, and T. B. Littenberg, Phys. Rev. D **76**, 083006 (2007).
96 M. C. Digman, and N. J. Cornish, Phys. Rev. D **108**, 023022 (2023).
97 H. Wang, I. Harry, A. Nitz, and Y. M. Hu, Phys. Rev. D **109**, 063029 (2024).
98 X. T. Zhang, N. Korsakova, M. L. Chan, C. Messenger, and Y. M. Hu, Phys. Rev. D **110**, 103034 (2024).
99 Y. Fu, Y. Wang, and S. D. Mohanty, Phys. Rev. D **111**, 043026 (2025).
100 Amaro-Seoane P, Schutz B F, and Thornburg J, arXiv: 1102.3647.
101 T. Hinderer, and É. É. Flanagan, Phys. Rev. D **78**, 064028 (2008).
102 L. Barack, and C. Cutler, Phys. Rev. D **69**, 082005 (2004).
103 S. Babak, H. Fang, J. R. Gair, K. Glampedakis, and S. A. Hughes,

Phys. Rev. D **75**, 024005 (2007).
104 A. J. K. Chua, and J. R. Gair, Class. Quantum Grav. **32**, 232002 (2015).
105 A. J. K. Chua, C. J. Moore, and J. R. Gair, Phys. Rev. D **96**, 044005 (2017).
106 M. L. Katz, A. J. K. Chua, L. Speri, N. Warburton, and S. A. Hughes, Phys. Rev. D **104**, 064047 (2021).
107 A. J. K. Chua, M. L. Katz, N. Warburton, and S. A. Hughes, Phys. Rev. Lett. **126**, 051102 (2021).
108 L. Barack, and A. Pound, Rep. Prog. Phys. **82**, 016904 (2019).
109 J. R. Gair, E. Porter, S. Babak, and L. Barack, Class. Quantum Grav. **25**, 184030 (2008).
110 J. R. Gair, C. Tang, and M. Volonteri, Phys. Rev. D **81**, 104014 (2010).
111 C. L. MacLeod, and C. J. Hogan, Phys. Rev. D **77**, 043512 (2008).
112 L. Barack, and C. Cutler, Phys. Rev. D **75**, 042003 (2007).
113 Q. Yun, W. B. Han, Y. Y. Guo, H. Wang, and M. Du, Sci. China-Phys. Mech. Astron. **68**, 210413 (2025).
114 C. Q. Ye, H. M. Fan, A. Torres-Orjuela, J. Zhang, and Y. M. Hu, Phys. Rev. D **109**, 124034 (2024).
115 X. Chen, Distortion of Gravitational-Wave Signals by Astrophysical Environments, edited by C. Bambi, S. Katsanevas, and K. D. Kokkotas, *Handbook of Gravitational Wave Astronomy* (Springer, Singapore, 2020), 1-12.
116 M. Sereno, A. Sesana, A. Bleuler, P. Jetzer, M. Volonteri, and M. C. Begelman, Phys. Rev. Lett. **105**, 251101 (2010).
117 R. Takahashi, and T. Nakamura, Astrophys. J. **595**, 1039 (2003).
118 X. Lin, J. Zhang, L. Dai, S. J. Huang, and J. Mei, Phys. Rev. D **108**, 064020 (2023).
119 Z. Cao, L. F. Li, and Y. Wang, Phys. Rev. D **90**, 062003 (2014).
120 M. R. Adams, and N. J. Cornish, Phys. Rev. D **89**, 022001 (2014).
121 C. Caprini, D. G. Figueroa, R. Flauger, G. Nardini, M. Peloso, M. Pieroni, A. Ricciardone and G. Tasinato, J. Cosmol. Astropart. Phys. **2019**, 017 (2019).
122 R. Flauger, N. Karnesis, G. Nardini, M. Pieroni, A. Ricciardone, and J. Torrado, J. Cosmol. Astropart. Phys. **2021**, 059 (2021).
123 E. Savalle, J. Gair, L. Speri, and S. Babak, Phys. Rev. D **106**, 022003 (2022).
124 B. P. Abbott, R. Abbott, T. D. Abbott, S. Abraham, F. Acernese, K. Ackley, C. Adams, V. B. Adya, C. Affeldt, M. Agathos, et al., Class. Quantum Grav. **37**, 055002 (2020).
125 I. Fiori, F. Paoletti, M. C. Tringali, K. Janssens, C. Karathanasis, A. Menéndez-Vázquez, A. Romero-Rodríguez, R. Sugimoto, T. Washimi, V. Boschi, et al., Galaxies **8**, 82 (2020).
126 F. Pozzoli, R. Buscicchio, C. J. Moore, F. Haardt, and A. Sesana, Phys. Rev. D **109**, 083029 (2024).
127 R. Rosati, and T. B. Littenberg, arXiv: 2410.17180.
128 G. Boileau, A. Lamberts, N. Christensen, N. J. Cornish, and R. Meyer, Mon. Not. R. Astron. Soc. **508**, 803 (2021).
129 T. B. Littenberg, and N. J. Cornish, Phys. Rev. D **91**, 084034 (2015).
130 T. A. Prince, M. Tinto, S. L. Larson, and J. W. Armstrong, Phys. Rev. D **66**, 122002 (2002).
131 G. Wang, and W. T. Ni, Phys. Scr. **98**, 075005 (2023).
132 M. Muratore, D. Vetrugno, S. Vitale, and O. Hartwig, Phys. Rev. D **105**, 023009 (2022).
133 M. Muratore, O. Hartwig, D. Vetrugno, S. Vitale, and W. J. Weber, Phys. Rev. D **107**, 082004 (2023).
134 G. Wang, B. Li, P. Xu, and X. Fan, Phys. Rev. D **106**, 044054 (2022).
135 O. Hartwig, and M. Muratore, Phys. Rev. D **105**, 062006 (2022).
136 P. P. Wang, X. Y. Lu, X. L. Zhao, H. K. Chen, J. Zhou, W. Huang, Y. J. Tan, H. Z. Wu, and C. G. Shao, Results Phys. **58**, 107481 (2024).
137 G. Wang, Phys. Rev. D **110**, 042005 (2024).
138 G. Wang, Phys. Rev. D **110**, 064085 (2024).
139 G. Wang, arXiv: 2502.03983.
140 N. Peterseim, *TWANGS — High-Frequency Disturbing Signals in 10 Hz Accelerometer Data of The GRACE Satellites*. Dissertation for the Doctoral Degree (Technical University of Munich, Munich, 2014).
141 M. Armano, H. Audley, J. Baird, P. Binetruy, M. Born, D. Bortoluzzi, E. Castelli, A. Cavalleri, A. Cesarini, V. Chiavegato, et al., Phys. Rev. D **106**, 062001 (2022).
142 T. Robson, and N. J. Cornish, Phys. Rev. D **99**, 024019 (2019).
143 A. Spadaro, R. Buscicchio, D. Vetrugno, A. Klein, D. Gerosa, S. Vitale, R. Dolesi, W. J. Weber, and M. Colpi, Phys. Rev. D **108**, 123029 (2023).
144 M. Colpi, K. Danzmann, M. Hewitson, K. Holley-Bockelmann, P. Jetzer, G. Nelemans, A. Petiteau, D. Shoemaker, C. Sopuerta, R. Stebbins, et al., arXiv: 2402.07571.
145 O. Burke, S. Marsat, J. R. Gair, and M. L. Katz, arXiv: 2502.17426, 2025.
146 P. Amaro Seoane, M. Arca Sedda, S. Babak, C. P. L. Berry, E. Berti, G. Bertone, D. Blas, T. Bogdanović, M. Bonetti, K. Breivik, et al., Gen Relativ Gravit **54**, 3 (2022).
147 J. Carré, and E. K. Porter, arXiv: 1010.1641.
148 Q. Baghi, J. I. Thorpe, J. Slutsky, J. Baker, T. D. Canton, N. Korsakova, and N. Karnesis, Phys. Rev. D **100**, 022003 (2019).
149 K. Dey, N. Karnesis, A. Toubiana, E. Barausse, N. Korsakova, Q. Baghi, and S. Basak, Phys. Rev. D **104**, 044035 (2021).
150 S. Lin, B. Hu, X. H. Zhang, and Y. X. Liu, Sci. China-Phys. Mech. Astron. **66**, 299512 (2023).
151 M. Armano, H. Audley, G. Auger, J. T. Baird, M. Bassan, P. Binetruy, M. Born, D. Bortoluzzi, N. Brandt, M. Caleno, et al., Phys. Rev. Lett. **116**, 231101 (2016).
152 M. Armano, H. Audley, J. Baird, P. Binetruy, M. Born, D. Bortoluzzi, E. Castelli, A. Cavalleri, A. Cesarini, A. M. Cruise, et al., Phys. Rev. D **97**, 122002 (2018).
153 M. Armano, H. Audley, J. Baird, P. Binetruy, M. Born, D. Bortoluzzi, E. Castelli, A. Cavalleri, A. Cesarini, A. M. Cruise, et al., Phys. Rev. Lett. **120**, 061101 (2018).
154 P. Whittle, J. R. Stat. Soc. Ser. B-Stat. Methodol. **20**, 334 (2018).
155 N. J. Cornish, Phys. Rev. D **102**, 124038 (2020).
156 J. R. Gair, F. Feroz, S. Babak, P. Graff, M. P. Hobson, A. Petiteau, and E. K. Porter, J. Phys.-Conf. Ser. **228**, 012010 (2010).
157 N. J. Cornish, and J. Crowder, Phys. Rev. D **72**, 043005 (2005).
158 X. H. Zhang, S. D. Mohanty, X. B. Zou, and Y. X. Liu, Phys. Rev. D **104**, 024023 (2021).
159 P. Gao, X. L. Fan, Z. J. Cao, and X. H. Zhang, Phys. Rev. D **107**, 123029 (2023).
160 W. D. Vousden, W. M. Farr, and I. Mandel, Mon. Not. R. Astron. Soc. **455**, 1919 (2016).
161 P. J. Green, Biometrika **82**, 711 (1995).
162 J. Kennedy, and R. Eberhart, in *Particle swarm optimization*: *Proceedings of ICNN'95 - International Conference on Neural Networks*, Perth, IEEE, 1995.
163 R. Storn, and K. Price, J. Glob. Optim. **11**, 341, (1997).
164 M. L. Katz, S. Marsat, A. J. K. Chua, S. Babak, and S. L. Larson, Phys. Rev. D **102**, 023033 (2020).
165 M. L. Katz, Phys. Rev. D **105**, 044055 (2022).
166 M. L. Katz, C. Danielski, N. Karnesis, V. Korol, N. Tamanini, N. J. Cornish, and T. B. Littenberg, Mon. Not. R. Astron. Soc. **517**, 697 (2022).
167 T. Robson, N. J. Cornish, N. Tamanini, and S. Toonen, Phys. Rev. D **98**, 064012 (2018).
168 M. S. Hartig, S. Paczkowski, M. Hewitson, G. Heinzel, and G. Wanner, Phys. Rev. D **111**, 043048 (2025).
169 H. Liu, Z. Luo, and G. Jin, Microgravity Sci. Technol. **30**, 775 (2018).
170 Q.-T. Zhang, H.-S. Liu, and Z.-R. Luo, Chin. Optics **16**, 1089 (2023).
171 O. Gerberding, B. Sheard, I. Bykov, J. Kullmann, J. J. E. Delgado, K. Danzmann, and G. Heinzel, Class. Quantum Grav. **30**, 235029 (2013).
172 J. B. Bayle, and O. Hartwig, Phys. Rev. D **107**, 083019 (2023).
173 Taiji Data Challenge II Manual, 2025, http://gr.imech.ac.cn/documents.
174 A. Klein, E. Barausse, A. Sesana, A. Petiteau, E. Berti, S. Babak, J.

Gair, S. Aoudia, I. Hinder, F. Ohme, et al., Phys. Rev. D **93**, 024003 (2016).
175 LISA Collaboration, LISA Verification Binaries GitLab repository, 2024, https://gitlab.in2p3.fr/LISA/lisa-verification-binaries.
176 T. Kupfer, V. Korol, T. B. Littenberg, S. Shah, E. Savalle, P. J. Groot, T. R. Marsh, M. Le Jeune, G. Nelemans, A. F. Pala, et al., Astrophys. J. **963**, 100 (2024).
177 V. Korol, N. Hallakoun, S. Toonen, and N. Karnesis, Mon. Not. R. Astron. Soc. **511**, 5936 (2022).
178 N. Karnesis, S. Babak, M. Pieroni, N. Cornish, and T. Littenberg, Phys. Rev. D **104**, 043019 (2021).
179 S. Khan, S. Husa, M. Hannam, F. Ohme, M. Pürrer, X. J. Forteza, and A. Bohé, Phys. Rev. D **93**, 044007 (2016).
180 A. Nitz, I. Harry, D. Brown, C. M. Biwer, J. Willis, T. D. Canton, C. Capano, T. Dent, L. Pekowsky, G. S. C. Davies, et al., PyCBC: A Python toolkit for gravitational wave data analysis, 2024, https://doi.org/10.5281/zenodo.10473621.
181 García-Quirós C, Tiwari S, and Babak S. PhenomT waveform model for LISA, arXiv: 2501.08261.
182 H. Estellés, A. Ramos-Buades, S. Husa, C. García-Quirós, M. Colleoni, L. Haegel, and R. Jaume, Phys. Rev. D **103**, 124060 (2021).
183 A. Gamboa, A. Buonanno, R. Enficiaud, M. Khalil, A. Ramos-Buades, L. Pompili, H. Estells, M. Boyle, L. E. Kidder, H. P. Pfeiffer, et al., arXiv: 2412.12823.
184 Pyseobnr: A Python package for SEOBNR waveforms, (2003). https://waveforms.docs.ligo.org/software/pyseobnr/index.html.
185 P. Shen, W. B. Han, C. Zhang, S. C. Yang, X. Y. Zhong, Y. Jiang, and Q. Cui, Phys. Rev. D **108**, 064015 (2023).
186 P. Shen, Q. Cui, and W. B. Han, Phys. Rev. D **111**, 024004 (2025).
187 X. Chen, and W. B. Han, Commun. Phys. **1**, 53 (2018).
188 Y. Jiang, W. B. Han, X. Y. Zhong, P. Shen, Z. R. Luo, and Y. L. Wu, Eur. Phys. J. C **84**, 478 (2024).
189 LISA Data Challenge Working Group, LISA Data Challenge Manual: Radler, 2020, https://lisa-ldc.lal.in2p3.fr/static/data/pdf/LDC-manual-002.pdf.
190 G. Wang, and W. T. Ni, Res. Astron. Astrophys. **19**, 058 (2019).
191 LISA Data Challenge Working Group, LISA Data Challenge Manual: Spritz, 2022, https://lisa-ldc.lal.in2p3.fr/static/data/pdf/LDC-manual-Spritz.pdf.
192 CosmoStatGW Collaboration, WF4Py: Waveforms for Python, year, https://github.com/CosmoStatGW/WF4Py.
193 F. Iacovelli, M. Mancarella, S. Foffa, and M. Maggiore, Astrophys. J. **941**, 208 (2022).
194 F. Iacovelli, M. Mancarella, S. Foffa, and M. Maggiore, Astrophys. J. Suppl. Ser. **263**, 2 (2022).
195 M. L. Katz, BBHx: Black hole binary waveforms for LISA, 2021, https://doi.org/10.5281/zenodo.5730688.
196 M. L. Katz, GBGPU: GPU-accelerated galactic binary analysis, 2022, https://doi.org/10.5281/zenodo.6500434.
197 Z. Wang, T. Yu, Y. Zhao, Z. Luo, W. Sha, C. Fang, Y. Wang, S. Wang, K. Qi, Y. Wang, et al., Photonic Sens. **10**, 265 (2020).
198 C. P. Sasso, G. Mana, and S. Mottini, Class. Quantum Grav. **36**, 075015 (2019).
199 J. N. Reinhardt, P. Euringer, O. Hartwig, G. Hechenblaikner, G. Heinzel, and K. Yamamoto, Phys. Rev. D **110**, 082005 (2024).
200 M. Staab, M. Lilley, J. B. Bayle, and O. Hartwig, Phys. Rev. D **109**, 043040 (2024).
201 J. B. Bayle, M. Lilley, A. Petiteau, and H. Halloin, Phys. Rev. D **99**, 084023 (2019).
202 N. Karnesis, M. L. Katz, N. Korsakova, J. R. Gair, and N. Stergioulas, Mon. Not. R. Astron. Soc. **526**, 4814 (2023).
203 M. Katz, N. Karnesis, N. Korsakova, Eryn: LISA parameter estimation software, 2023, https://doi.org/10.5281/zenodo.7705496.
204 D. Foreman-Mackey, D. W. Hogg, D. Lang, and J. Goodman, Publ. Astron. Soc. Pac. **125**, 306 (2013).

Appendix Parameter estimation of verification binary dataset with a "noise agnostic" workflow

In this appendix, we showcase a simple parameter estimation task on dataset 0.1, illustrating the basic utility of TDC II data and validating the fidelity of our simulations. The data is composed of 55 VGB signals and instrumental noises. As discussed in Section 3.2, we are very likely to face a situation where noise characteristics can not be known priorly. To account for this scenario, our analysis is conducted based on a "noise-agnostic" workflow (Figure a1). After suppressing laser frequency noises via the 2nd-generation Michelson TDI combinations, we analyze a narrow frequency bin of width $O(10^{-6})$ Hz around each signal, and utilize data at the adjacent frequency bands to evaluate the PSD via the Welch method. The mean PSD of these bands is adopted as the noise floor (ignoring the spectral shape due to the narrow bandwidth). Now we are ready to compute the likelihood function using `Triangle-GB` and generate posterior samples with PTMCMC implemented in the `Eryn` [202-204] sampler. Conservative hyperparameters (`n_walker`=200, `n_temp`=10) are chosen, and an affine invariant proposal is used to minimize tuning.

The full posterior distributions for 1 VGB and the sky localizations of the other 9 randomly selected VGBs are shown in Figure a2. Note that our simulation spans only one year, while the "detectable" GBs [176] are defined based on 48-month observation. Consequently, the last signal exhibits a low total SNR ($\lesssim 7$), which is faithfully reflected in its posterior distribution (i.e., the localization is poorly constrained).

Figure a1 (Color online) The "noise-agnostic" workflow implemented on the verification binary dataset.

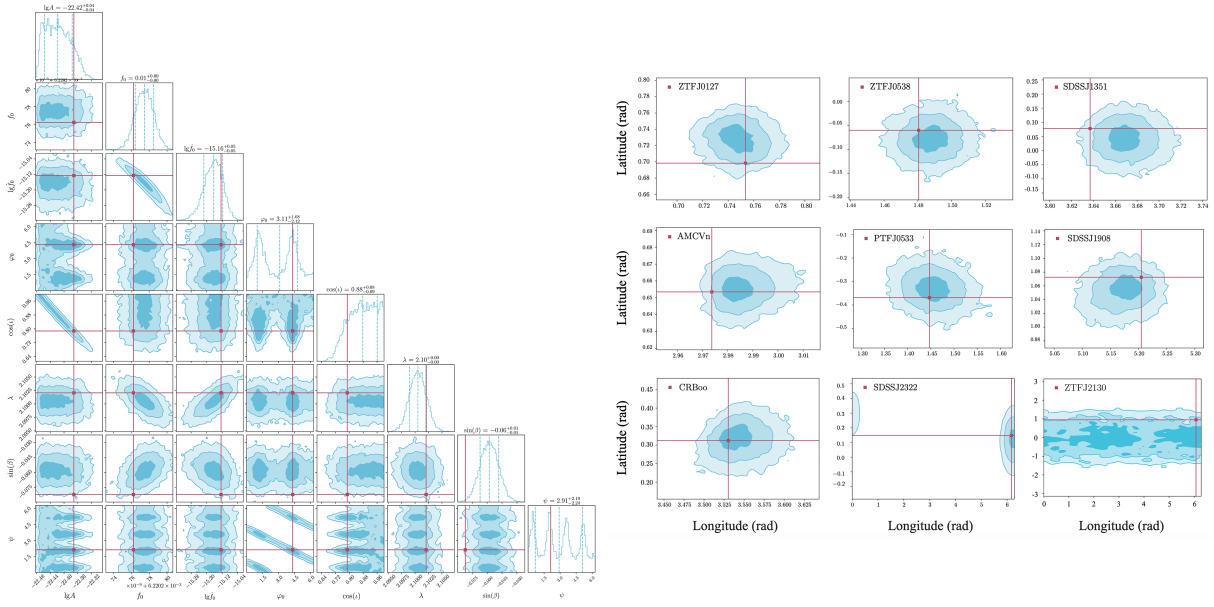

Figure a2 (Color online) Left 1 panel: the full posterior distributions for 1 VGB. Right 9 panels: the sky localizations of the other 9 VGBs, with the x-axis and y-axis representing the Ecliptic longitude and latitude, respectively.